Blood velocities estimation using ultrasound

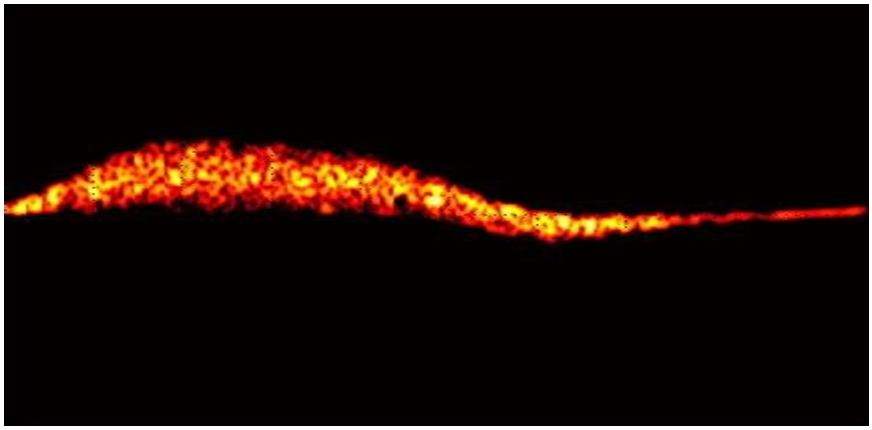

Elham Pirnia

Supervised by: **Andreas Jakobsson**
Examiner: **Maria Sandsten**

Center for Mathematical Science, Mathematical Statistics
Lund University, Sweden
September 2013

Abstract

This thesis consists of two parts. In the first part, the iterative data-adaptive BIAA spectral estimation technique was extended to estimate lateral blood velocities using ultrasound scanners. The BIAA method makes no assumption on samples depth or sampling pattern, and therefore allows for transmission in duplex mode imaging. The technique was examined on a realistic Field II simulation data set, and showed fewer spectral artifacts in comparison with other techniques. In the second part of the thesis, another common problem in blood velocity estimation has been investigated, namely strong backscattered signals from stationary echoes. Two methods have been tested to examine the possibility of overcoming this problem. However, neither of these methods resulted in a better estimation of the blood velocities, most likely as the clutter characteristics in color flow images vary too rapidly to allow for this form of models. This might be a result of the non-stationary tissue motions which could be caused by a variety of factors, such as cardiac activities, respiration, transducer/patient movement, or a combination of them.

Acknowledgements

I wish to thank my supervisor *Professor Andreas Jakobsson* at the at Department of Mathematical Statistics at Lund University, whom without his inspiring ideas and support, it would have been impossible to write this thesis.
I also like to thank *Erik Gudmunson* and *Johan Swärd* who kindly helped me throughout the thesis and shared their knowledge and codes to help me understand related concepts.
I would like to thank *Professor Jørgen Arendt Jensen* from Technical University of Denmark, who kindly shared his codes and data with me. Moreover, I would like to thank all *my friends and the staff* in Department of Mathematical statistic in Lund university for their support and motivation during the time I have spent in Lund, in particular, *James Hakim* who helped me with technical issues.
Also, I would like to thank my parents *Goli* and *Reza* and my siblings *Arash* and *Anahita* who have always been such a great advisers for me, during my whole life, and supported me through every situations.
And last but not the least, I would like to thank my husband, *Kian Skandarioon*, who always supported me and motivated me throughout my studies.

CONTENTS

Chapter 1

INTRODUCTION

The cardiovascular system, which is responsible for carrying oxygen and nourishment to the organs, generates a complex flow pattern which cause velocity changes throughout this system. This system has been investigated in different manners to visualize inner body parts. The main system that allows for noninvasive examination of cardiovascular system is ultrasound [1, 2], which is painless and safe for the patient and can make rapid diagnosis possible. Conventional Doppler ultrasound systems are limited by angle-dependent and one-dimensional velocity estimation, that cannot show the complexity of blood flow in the body. To overcome the angle dependency in conventional Doppler systems, many methods have been suggested, to calculate the two-dimensional vector of velocity. [3–7]. Here, we will examine a particular solution developed by Jensen and Munk [8, 9], where they use a transverse oscillation (TO) method for calculating the two-dimensional vector velocity; this idea has also been suggested by Anderson [10, 11].

The method introduces two double oscillations in ultrasound beams, each 90^0 transverse phase shifted in space [12]. TO has previously been tested both with simulated flow and in-vivo data [12–15]. Moreover, Hansen et al. have investigated feasibility of vector flow estimation, by using TO directly on the heart, in-vivo, during surgery, to provide examples of vector flow measurement of different cardiac sites and to compare the measurements to conventional Doppler ultrasound [**?**].

Estimation of power spectral density (PSD) of the sampled signal is a common way to estimate the blood velocity at a specific depth. Displaying this PSD as a function of time, a so-called sonogram or spectrogram, displays the changes in the blood velocity distribution over time. Conventional ultrasound systems, estimate PSD by using the periodogram estimator or Welch's method. However, this approach suffers from low resolution and/or high leakage [16]. Therefore to achieve adequate spectral resolution, the number of observed samples should be large. This means that a large number of transmissions has to be used to estimate the PSD, which cause a reduction in resolution. Furthermore, in color flow imaging, where B-mode images will be generated along with spectograms, it is also necessary to be able to investigate the region in which the blood velocity will be estimated. As the same system is used for both the velocity estimation and for forming B-mode images, these two transmissions are interleaved, and since B-mode images should

be update frequently to allow the user to find and track the position of the vessel, it is necessary to reduce the number of Doppler transmissions in order to use the next part of the transmissions for generating B-mode images [2].

Another common problem in blood velocity estimation is the backscattered signals from vessel's walls and surrounding tissues (such as bones). The strength of theses signals, which here will be referred to as stationary echos, clutters or inferences, are typically 40 to 60 dB larger than the desired flow signal, which may easily corrupt the flow velocity estimates [17]. Thus, effectively removing the clutter is essential for accurate velocity estimations.

In this thesis, making use of the work done in [8] and [18], an iterative data-adaptive blood velocity spectral estimator is introduced. This estimator that allows for an arbitrary sampling of measurements over emission, is used to estimate the transversal blood velocity, and realistic Field II [19] simulated data was applied to examine the performance of the technique. Afterwards, making use of proposed algorithms in [20] and [21], two different ways have been tried to suppress/remove the backscattered signals from stationary echos, and the performance of the proposed algorithms have been tested on the in-vivo data [22].

The thesis is outlined as follow: In *Chapter 2*, some basic concepts about ultrasound imaging, blood flow, and medical ultrasound imaging will be introduced. *Chapter 3* presents the conventional blood velocity estimation (1D blood velocity estimation) and the TO technique for 2D blood velocity estimation. *Chapter 4* covers the filter bank power spectral estimation methods and the BIAA estimator is detailed. In *Chapter 5*, the performance of the proposed algorithm are examined. In *Chapter 6* two different algorithms to suppress/remove the clutters are introduced and their performance are tried on in-vivo data measured from the carotid arteries.

Chapter 2

BACKGROUND

In the first part of this chapter, some basic concepts in ultrasound imaging are described. After that, a brief description of the human circularity and blood flow is explained. Finally some medical ultrasound system is mentioned.

2.1 Ultrasonic imaging

Ultrasonic imaging covers the whole area that sound waves of above 20 KHz (the audible range for humans) are used to produce images, and for medical applications the frequency range is from 1 to 10 MHz. Typically, for intra-vascular imaging, frequencies up to 50 KHz are used. Ultrasounds are of great use in medicine, since they can be used to generate images of human tissues non-invasively and the speed of the sound (1,540 m/s for human tissue) makes it possible to have real-time images of the human body. Ultrasonic imaging resulted in many techniques, one of them is called pulse-echo mapping, that is the base of development of new velocity estimators. Pulse-echo technique was first used during World War I in sonar systems and it's pioneer use in medical application goes back to early 1950s. In this technique, a pulsed pressure field is generated by piezoelectric transducer and emitted to the tissue, the propagated field is then partly reflected from tissue, the back-scattered signal is received by same/other transducer and then it will used for different applications [23].

2.1.1 Ultrasound waves

Ultrasound is a mechanical vibration, and no mass is transported during the propagation of the wave. The particles of the medium crossed by the ultrasounds just oscillate around their mean positions, instead of being at rest and equally spaced as before the disturbance. Figure 2.1 shows propagation of a plane wave. The oscillation will be along the direction of the wave making it longitudinal and the disturbance will propagate with speed c, which depends on the medium and is given by

$$c = \sqrt{\frac{1}{\rho_0 \kappa}}$$

where ρ_0 is mean density and κ is the adiabatic compressiblity[1]. In medical ultrasound most of the time the propagation is linear [2] and this is always assumed to hold in this thesis.

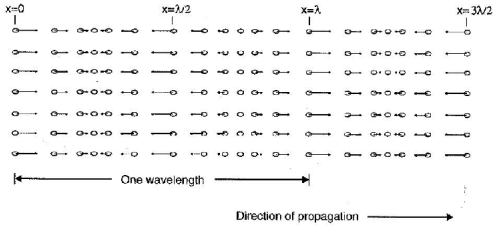

Figure 2.1. Particle displacement for a propagating ultrasound wave. Figure from [2].

2.1.2 Scattering

A wave which propagates through a medium continues straight in the same direction until it crosses a new medium. When this happens, part of the wave is transmitted through the new medium, probably changing direction, while part of it is reflected back [2]. This is called scattering.

2.1.3 Attenuation

The ultrasound wave propagated in tissue will be attenuated because of absorption and scattering. The dependence between attenuation and distance traveled and frequency is often linear. Attenuation in tissue is due to both scattering, which will spread energy in all directions, and absorption, which converts it into thermal energy [2].

2.1.4 Transducer

The acoustic pressure field emitted into the tissue is generated by an ultrasound transducer. There are different transducers with different constructions. In blood flow imaging, array transducers are used. The most common types of arrays are shown in Figure 2.2 [2].
A piezoelectric crystal is located at one end in the transducer. This crystal, when energized, transmits ultrasound waves toward flowing blood. A part of the sound will be reflected by the red blood cells. The reflected ultrasound waves travels backward to the crystal. The frequencies of these reflected waves are lower frequency

[1] Adiabitic process is any process that occurs without gain or loss of heat.

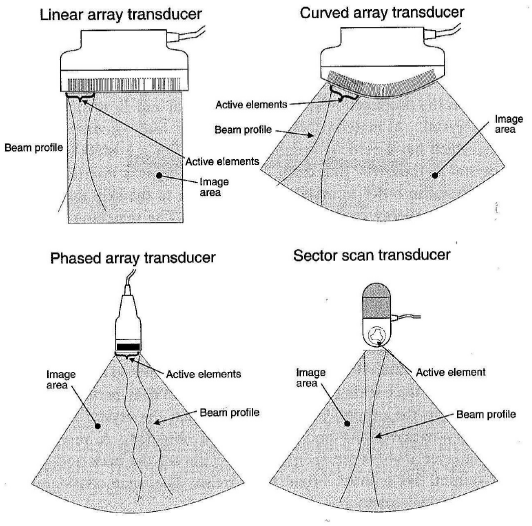

Figure 2.2. Different ultrasound transducers for acquiring B-mode images. Figure from [2].

than the transmitted wave, since the red cells are moving away from the transmitter crystal. To compensate this, they are amplified by transducer and then frequency difference between the transmitted wave and the reflected wave is determined, and the velocity of blood flow will be determined [24].

2.2 Flow physics

In this section, some basic concepts of human circularity and physics of blood flow are introduced, to give the reader a better understanding of circularity system.

2.2.1 Human circularity system

Human circularity system is responsible for carrying oxygen and nourishment to organs and disposing the waste products resulting from metabolism, and it consists of

- Heart: Which is responsible for pumping action of blood into aorta.
- Blood: which is made of two parts:
  - Plasma: which makes up 55 percent of blood volume.
  - Formed cellular elements (red and white blood cells, and platelets) which combine to make the remaining 45 percent of blood volume.

- Blood vessels: The blood vessels are the part of the cardiovascular system that transports blood throughout the body. There are three major types of blood vessels
  - Arteries: the function of the arteries is to transport blood under high pressure to the tissues, therefore, the arteries have strong vascular walls, and blood flows at a high velocity in the arteries.
  - Capillaries: which enable the actual exchange of water and chemicals between the blood and the tissues. To have this role, the capillary walls are very thin.
  - Veins: which carry blood from the capillaries back toward the heart, they are a major reservoir of extra blood. The pressure in the venous system is very low, therefore venous walls are thin.

2.2.2 Blood pressure

Blood pressure, which is the measurement of force that is applied to the walls of the blood vessels is high in aorta (averaging about 100 mm Hg[2]), because the heart pumps blood continually into the aorta. Also, because heart pumping is pulsatile, the arterial pressure alternates between a maximum (systolic) pressure level of 120 mm Hg and a minimum (diastolic) pressure level of 80 mm Hg[3].

The pressure in capillaries varies from as high as 35 mm Hg to as low as 10 mm Hg. But these levels can change according to the age and situation of body [24]. Table 2.1. shows a normal range of blood pressure for a normal person in aorta.

Table 2.1. Desired blood pressure in a normal person

systolic, mmHg	diastolic, mmHg
90-119	60-79

2.2.3 Blood flow

Blood flow, which is the quantity of blood that passes a given point in the circulation in a given period of time through a blood vessel, is pulsating and it has very complex flow pattern. It is determined by two factors:

1. Pressure difference between two ends of the vessel, which is the force that pushes the blood through the vessel

[2]Blood pressure almost always is measured in millimeters of mercury (mm Hg) because the mercury manometer has been used as a reference for measuring pressure. When one says that the pressure in a vessel is 50 mm Hg, it means that the force applied is enough to push a column of mercury against gravity up to a level 50 mm high [24].

[3]The cardiac cycle consists of a period of relaxation called diastole, during which the heart fills with blood, followed by a period of contraction called systole [24].

2. Vascular resistance.

The flow through the vessel can be calculated by Ohm's law:

$$F = \frac{\Delta P}{R}$$

in which F is blood flow, ΔP is the pressure difference ($P1 - P2$) between the two ends of the vessel, and R is the resistance.

Many mechanical devices can be used to measure the flow. They are called flowmeters, which can be used both inside and outside of vessels. Ultrasound is one of the flowmeters that can be used outside the vessel to measure the flow. Pressure has a great effect on blood flow, because an increase in arterial pressure, not only increases the force that pushes blood through the vessels but also swells the vessels at the same time, which decreases vascular resistance. Thus, greater pressure increases the flow in both of these ways. Therefore, blood flow at 100 mm Hg arterial pressure is usually four to six times as great as blood flow at 50 mm Hg instead of two times [24].

2.2.4 Pathological conditions

The normal pulsatile flow of blood can be disturbed by some pathological conditions, such as cancer, or formation of plaque within vessels which evolves with age in humans. The cancer cells or plaque change the flow conditions. The blood velocity increases when the cross-sectional area gets smaller. These are only two of many conditions that may change the pulsatile flow in body and can be diagnosed by using ultrasound and the velocity estimations [2].

2.2.5 Stationary echoes

Stationary echoes are the signals coming from vessel boundaries and tissues around them. These factors are larger than the signal coming from the blood and it is necessary to remove/suppress them, to avoid corruption of the blood velocities estimates. A solution to reduce these disturbances may be found by inserting a high pass filter; however, this may then also effect the low velocity estimation, which is important in the diagnose of some diseases [2].

2.3 Medical Ultrasound systems

The field of medical ultrasound has developed since its first use and it caused the development of ultrasound systems, from systems that acquire single lines of data to today's imaging systems which are capable of displaying anatomic gray scale images as well as blood flow maps in real time [2]. Description of the most prominent ultrasound systems are given in this section.

2.3.1 Gray scale ultrasound systems

In this system, the amplitude of the back-scattered signal is shown as a A-line (Amplitude) on the screen, where height shows the reflection strength, and thus the differences in acoustic properties from the surroundings, and the horizontal axis shows the time, and is equivalent to the depth in tissue. But it is hard to see the the structure of organs, but on the other hand it would be easy to see the motion of the tissue and movement of heart [2]. The representation of the motion can be shown by displaying a number of A-lines side by side, which is called an M-mode (Motion) system, the amplitude of the the lines is shown by a gray value, so that large reflections are white. Figure 2.3 shows the M-mode image of heart valves.

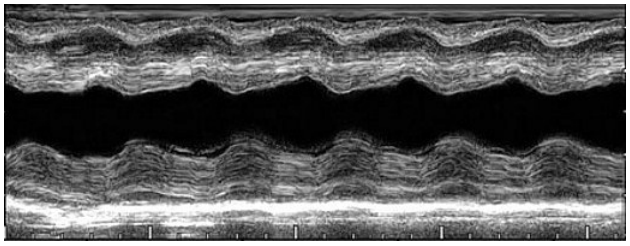

Figure 2.3. M-mode image of heart valves. Figure from [2].

A two dimensional image of tissue structure is obtained by so called B-mode (Brightness) systems, Figure 2.4 shows a gray-scale B-mode image of liver and kidney, where higher gray level shows higher reflection of the tissue at a given depth [2].

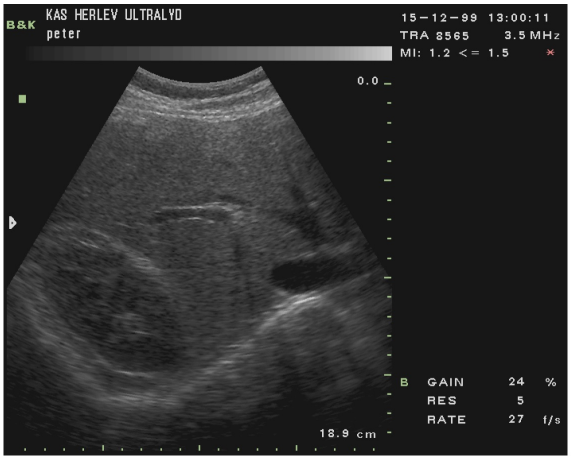

Figure 2.4. B-mode image of liver and kidney. Figure from [23].

Disadvantage of this method was that it needed a long time to make the image and images could not be seen clearly as a result of tissue motion.

2.3.2 Continuous wave systems

The earliest systems for studying blood flow, suggested by Satomura (1975), was a continuous wave (CW) system using the Doppler effect. This effect is named after Austrian physicist Christian Andreas Doppler (1803-1853), and describes the change in frequency that occurs when the source or target are in motion. So the received frequency for an observer will be

$$f_d = f_0 \frac{c + v_o}{c + v_s}$$

where f_0 is the original frequency, f_d is the received frequency for observer, v_0 is the speed of the observer, v_s is the speed of the source, and c is the speed of the sound. Since blood scatters ultrasound, Satomura was able to detect the velocity of flowing blood. To exploit the Doppler shift, one transducer continuously emits a sinusoidal ultrasound wave,

$$e(t) = cos(2\pi f_0 t)$$

which enters the tissue, and a second ultrasound receives the back-scattered waves,

$$r_s(t) = a\, cos(2\pi f_0 \alpha (t - t_0))$$

where

$$\alpha \approx 1 - \frac{2v_z}{c}$$

$$\alpha t_0 \approx \frac{2d_0}{c}$$

denoting with v_z the velocity along the direction z (the direction of the ultrasound beam) and d_0 the initial position of the scatters. Then the received signal will be multiplied by a quadrature signal of frequency f_0 to find the Doppler shift. Applying the Fourier transform, we get

$$r_s(t) \exp(j2\pi f_0 t) \leftrightarrow R_s(f - f_0)$$

where $R_s(f - f_0)$ is the Fourier transform of $r_s(t)$. Afterwards, a band pass filter is used, in order to remove both the components coming from the stationary tissue and the high frequency signals at twice the emitted signal. The remaining signal after filtering is:

$$m_f(t) \approx \frac{a}{2} \exp(j2\pi f_0 \frac{2v_z}{c} t) \exp(-j2\pi f_0 \alpha t_0)$$

where the second exponential term represents the delay caused by the round trip time between emission and reception. The resulting signal contains the Doppler shift of the emitted signal.

To image the vessel, a transducer is moved in two dimension over the region of interest, and when a significant excursion from f_0 appeared, a map of vessel will be shown. This kind of images are called C-scan. CW systems are still used in modern scanners as a supplement to the pulsed techniques, since aliasing errors are more easily controlled for a CW system [2].

2.3.3 Pulsed wave systems

Continuous wave system lacks the possibility of detection of the depth in tissue of the vessel when the two vessels are close to each other. So it is possible that two vessels, at different depths, unintentionally be insonified at the same time and, therefore, result in a wrong frequency estimation.
To remedy this, a pulsed wave system was suggested by Baker (1970) and others. In this method, a number of pulses are emitted into the tissue, and the back-scattered signal received by transducer is sampled at the same time relative to the pulse emission. Then this signal will be multiplied by the center frequency of the emitted pulse and will be low-pass filtered. The displacement of the backscattered signal, as a consequence of the movement of the blood, is then detected. These systems are also called Doppler systems which is a misleading since they do not use the Doppler effect. It is the shift in the position of the scatters, not shift in the emitted frequency that is detected. Figure 2.5 shows the received signal after demodulation and filtering; here, the depth in tissue is fixed and the signals are shown in the left side of the picture result from a sequence of pulses. Each line corresponds to a single pulse, and the different pulses are emitted at a pulse repetition frequency, f_{prf}. On the right side, instead, there is the resulting sampled signal, produced by taking into account the amplitude of each pulse after a fixed time (indicated by the dashed line in the left graph) [2].
Between two emission the scatter move a distance proportional to the velocity component v_z in the direction of ultrasound beam. The time shift t_s of the RF signal from pulse to pulse is

$$t_s = \frac{2v_z}{c} T_{prf}$$

where c is the speed of the sound, and T_{prf} is the time between pulse emissions. This movement can be measured by recording the signal at a specific depth. Taking out one sample at a specific depth for each line gives a sampled signal with a frequency proportional to the scatter velocity [23]. So if the transducer emits a sinusoidal pulse, the received sampled signal for ith pulse emission for a single scatter will be [2]

$$r(i) = a(i)sin(2\pi f_p i T_{prf} + \theta)$$

where

$$f_p = \frac{2v_z}{c} f0$$

and $a(i)$ is the amplitude, f_0 the emitted frequency, and θ a phase factor explaining the depth of interest.

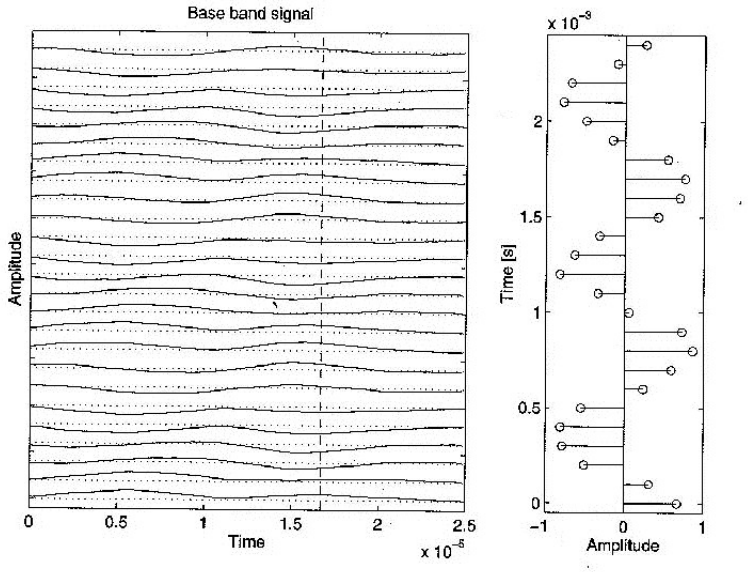

Figure 2.5. Sampling for a single range gate pulsed wave. The left graph shows the different received signals. A single pulse is emitted for each line and signals are displaced in amplitude to show them on the graph. The right graph shows the resulting sampled signal. Figure from [25].

This system made the investigation of one vessel more accurate, and moreover demonstration of velocity profiles became possible. Moreover, duplex mode imaging, i.e., displaying both B-mode image and blood velocity estimate became possible by using two transducers, or a multi-element transducer. Two-transducer systems are not used these days, since it is easier to use a multi-element transducer to generate a duplex image. Figure 2.6 shows a duplex scan showing both B-mode image and spectrogram of the carotid artery.

2.3.4 Color flow imaging

The first pulsed wave systems found the velocity by counting the number of zero-crossing per second, but in order for this to be accurate, one needs at least half a period of the received signal and a number of periods to be observed, which does not work well for displaying an image of the typically non-stationary blood flow. Estimators that can find the velocity by using only 2 to 10 RF lines instead of hundreds (in pulsed-wave systems) were developed in 1970s and 1980s. They find the velocity from changes in position of the received signal by estimating the phase shift (auto-correlation approach) or time shift (cross-correlation approach). Using

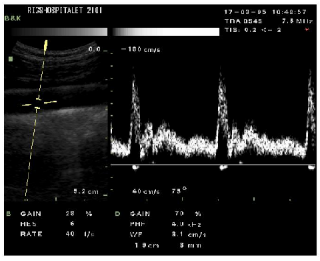

Figure 2.6. Duplex scan showing both B-mode image and spectrogram of the carotid artery. Figure from [2].

fewer RF lines makes it possible to get the flow profile and display them on top of a B-mode image. To differentiate flow direction, usually red color is selected for flow in arteries and blue color for veins. The brightness of color shows the magnitude of the velocity [2]. An example of CFM (Color Flow Mapping) is shown in Figure 2.7.

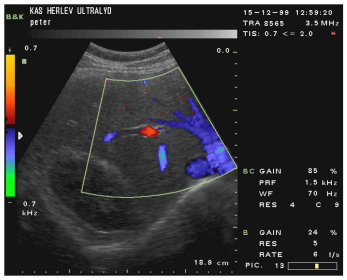

Figure 2.7. B-mode and CFM mode image of liver and kidney. Figure from [23].

Chapter 3

BLOOD VELOCITY ESTIMATION

Estimation of blood velocity using backscattered signal can be done in different ways. In this chapter, first the common methods to estimate the blood velocity are mentioned and then some difficulties and limitations are discussed. After that, the velocity estimation in one dimension is described. Finally, this chapter ends by the description of blood velocity estimation in two dimension.

3.1 Velocity estimators

Here, some of the methods which can be used to estimate the blood velocity profile from sampled signal, described in [25], are detailed.

3.1.1 Spectral estimator

The Fourier transform of the received signal can be used to show velocity distribution, since the frequency volume of the received signal is equivalent to the velocity distribution of the blood. The power spectral density (PSD) can be saved together to generate the spectrogram, which is also, incorrectly, being termed the Doppler spectrum. In order to do this, the received signal is divided into sections and the PSD is calculated for each of these sections. Then, the evolution of the velocity distribution can be observed by displaying these spectra side by side. Figure 3.1 shows the sonogram from an artery.
To display both positive and negative frequencies, a quadrature signal is employed. This is the technique which is used throughout this thesis.

3.1.2 Auto-correlation estimator

An alternative approach to estimate the blood velocity is to use an auto-correlation approach. The auto-correlation approach estimates the mean velocity of the scatters by estimating the mean phase shift from emission to emission [2], [26].

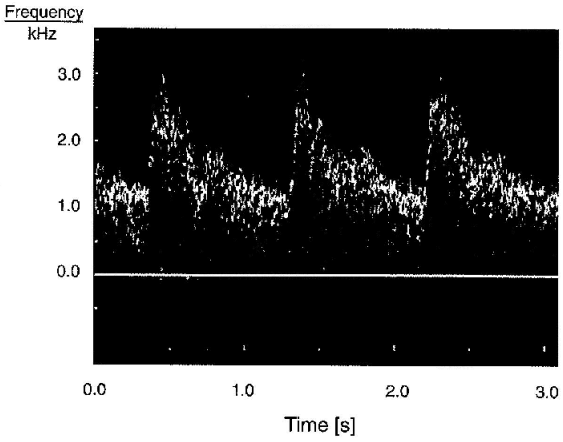

Figure 3.1. Sonogram (time-frequency) display of the Doppler signal from an artery. Figure from [2].

3.1.3 Cross-correlation estimator

Another way to estimate the velocity is to use a cross-correlation approach. The method is based on tracking the change in position of scatters from emission to emission. Dotti et al. [27] were the first to suggest such an approach. Also Bonnefous and Pesque [28] and Foster et al. [29] have helped on the development of the time-based cross-correlation method.

3.2 Clutter filtering

One major challenge with velocity estimation using ultrasound is the strong back-scattering from stationary echos. The normal scattering coefficient of blood is on the order of 10 to 100 times smaller than one from the vessel boundaries and the surrounding tissue. Consequently, the strong stationary echoes' signals must be removed, as otherwise they will corrupt the frequency estimations. This can for example be done by applying a high-pass filter. Although, commonly, this is done by subtracting out the mean of the signal [2]. In this project we have tried two novel alternatives to suppress/remove these clutters as will be further explained in chapter 6.

3.3 Velocity limitation

The received signal from one blood cell will have the same shape as the emitted pulse from the transducer, but it will be time scaled and, therefore, its frequency

will be different from the propagated pulse. The time shift between two RF lines is

$$t_s = \frac{2v_z}{c} T_{prf}$$

and it increases linearly with the line number i. The frequency of the received signal is $f_p = \frac{2v_z}{c} f_0$, which is a scaled version of f_0. So the spectrum of the received signal has the spectral shape of the pulse, with a scaled frequency axis.
To detect the velocity and distinguish the signal of interest from stationary echo, at least one period of the waveform should to be observed. Therefore, the lowest possible velocity can be found from equation:

$$NT_{prf} = \frac{c}{2v_{min} f_0} \tag{3.3.1}$$

implying that

$$v_{min} = \frac{c f_{prf}}{2N f_0} \tag{3.3.2}$$

and thus, the minimum frequency is $f_{min} = \frac{f_{prf}}{N}$. To avoid aliasing, the maximum velocity is determined by the pulse repetition frequency. Aliasing will occur for frequencies above the Nyquist frequency, $f_N = \frac{f_{pfr}}{2}$b [2]. To avoid this, we require that

$$\frac{f_{prf}}{2} \leq \frac{2v_{max}}{c} f_0$$

and thus are limited to estimating the maximum velocity

$$v_{max} = \frac{c}{2} \frac{f_{prf}}{2f_0}. \tag{3.3.3}$$

Higher velocities will cause aliasing.

3.4 1D velocity estimation

In conventional CFM systems, the velocity estimation is performed by emitting a pulsed sinusoidal ultrasound field, i.e., $p(t) = \cos(2\pi f_0 t)$, in one direction a number of times. The returned signal is then sampled at the depth of interest, d_0, see also Figure 3.2.
The sampled signal for a monochromatic wave with[1] an unit amplitude is given by

$$r(k,l) = \cos\left(2\pi(\frac{f_0}{f_s}k - \frac{2v_z}{c} f_0 l T_{prf})\right) \tag{3.4.1}$$

where c is the speed of the sound, v_z the axial blood velocity component along the ultrasound beam, f_0 the center frequency of transducer, l the slow time index (emission times), k the fast time index (sample depth), T_{prf} the time between pulse

[1] A monochromatic wave is a wave which has a single frequency.

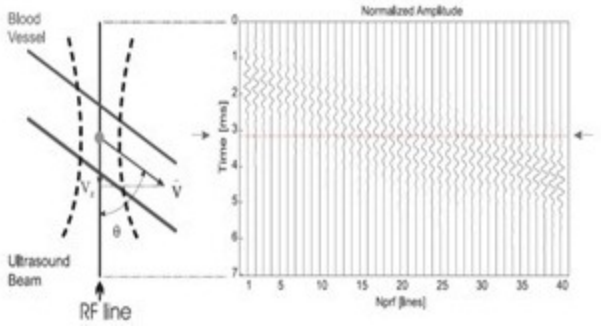

Figure 3.2. Consecutive received RF signals for a pulsed wave system with one scatter moving slowly past the range depth/gate indicated by dashed line at the arrows. Figure from [23].

emissions, f_s the sampling frequency, and $\Phi = 2\pi\frac{f_0}{f_s}$ is a phase factor that depends on the depth, d_0. The frequency of the returned signal

$$\psi = -2\pi\frac{2v_z f_0}{f_{prf}c} \tag{3.4.2}$$

is thus, proportional to the axial blood velocity component and can be found from either the mean frequency or the phase shift of the signal between pulse emissions [2]. To acquire both positive and negative velocities, a signal with a one-sided spectrum should be used, which can be found by performing a Hilbert transform of the signal. Then, the sampled signal would be:

$$r_q(k,l) = exp\left(j(\Phi k + \psi l)\right) \tag{3.4.3}$$

where

$$\Phi = 2\pi\frac{f_0}{f_s}$$

implying that the velocity at this depth can be estimated by one of the methods described in section 3.1.

3.4.1 Angle dependency problem

Conventional velocity estimators in ultrasound systems are only able to estimate the axial velocity component, v_z, along ultrasound beam. The axial velocity is

$$v_z = |v|cos\theta$$

where $|v|$ is the velocity magnitude. So such systems are angle dependent, and since most vessels in human body are parallel to the skin, this angle dependence is a main limitation in current ultrasound systems. That's why a lot of effort has been made to estimate the velocity vector in 2D and 3D [25].

3.5 2D velocity estimation

In section 3.4, estimation of blood velocities using ultrasound in one dimension was explained. However, in section 3.4.1 was stressed that this technique only allows for estimation of the velocity component along the ultrasound beam direction, ignoring the possible flow transverse to the beam direction, as is shown in Figure 3.3. This is of course a problem in estimation of blood velocities, since most vessels are parallel to the skin surface, besides, the flow in the vessel is not always parallel to the vessel surface [23].

Herein, the idea of Jensen and Munk [8], who suggested to introduce a transverse oscillation in the ultrasound beam, which would influence the received signal and thus permit to estimate both the axial and transverse velocity will be described.

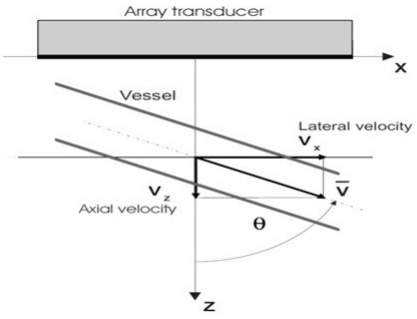

Figure 3.3. Coordinate system for blood particle moving through an ultrasound beam. Figure from [23].

In [9], Jensen has proposed a two-dimensional vector velocity estimator, so that it is possible to estimate both the axial and the transverse velocities of the flow at one depth of interest. The details of this estimator can be found in his paper, and here briefly. Using the same notation as (3.4.1) the sampled signal for a monochromatic, unit amplitude signal, used to estimate the axial velocity at a given depth, can be expressed as

$$r(k,l) = \cos\left(2\pi(\frac{f_0}{f_s}k - \frac{2v_z}{c}f_0 l T_{prf})\right) \tag{3.5.1}$$

where the indexes l and k indicate the slow and the fast time, respectively. Here, v_z is the axial velocity, i.e., the velocity along the beam direction. In order to be able to estimate the velocity also in the transverse direction, i.e., v_x, a transverse oscillation in the ultrasound beam (3.5.1) was introduced [9], so v_x influence the received signal as well. Then, the sampled signal for a given depth will be

$$r_t(k,l) = \cos(2\pi\frac{f_0}{f_s}k - 2\pi\frac{2v_z}{c}f_0 l T_{prf})cos(2\pi\frac{v_x}{dx}lT_{prf}). \tag{3.5.2}$$

Here dx indicates the lateral modulation period [23]. The frequency due to the transverse motion can then be written as

$$f_x^v = \frac{v_x}{dx} \tag{3.5.3}$$

By introducing

$$f_p^v = \frac{2v_z}{c} f_0 \tag{3.5.4}$$

and

$$\Phi = 2\pi \frac{f_0}{f_s}$$

one may rewrite (3.5.2) as

$$r_t(k,l) = \cos(\Phi k - 2\pi f_p^v l T_{prf}) cos(2\pi f_x^v l T_{prf}) \tag{3.5.5}$$

To obtain an one-sided spectrum, the Hilbert transform of the signal should be calculated. For axial velocity estimation the sampled signal is as (3.4.3). But a spatial Hilbert transform must be used to get a spatial quadrature signal in this case [9]. This should be done, first just in the direction transverse to the beam, so that the received and sampled spatial quadrature signal ($r_t + j\mathcal{H}_x\{r_t\}$) is expressed as:

$$r_{sq}(k,l) = \cos(\Phi k - 2\pi f_p^v l T_{prf}) exp(j2\pi f_x^v l T_{prf}) \tag{3.5.6}$$

The received field is, thus, influenced by both the axial and the transverse velocity, so to estimate v_x, the influence from the axial velocity should be compensated. Therefore, the method explained in [30] was used to generate two new signals as follow. By taking the temporal Hilbert transform of (3.5.6) but this time in direction of beam

$$r_{sqh}(k,l) = \sin(\Phi k - 2\pi f_p^v l T_{prf}) \exp(j2\pi f_x^v l T_{prf}) \tag{3.5.7}$$

is obtained. Then, by using Euler's formula,[2] (3.5.6) and (3.5.7) can, respectively, be written as

$$\begin{aligned} r_{sq}(k,l) = \frac{1}{2}\{\exp(j\Phi k - j2\pi f_p^v l T_{prf}) + \exp(-j\Phi k + j2\pi f_p^v l T_{prf})\} \\ \times \exp(j2\pi f_x^v l T_{prf}) = \frac{1}{2}\exp\{j2\pi(f_x^v - f_p^v) l T_{prf} + j\Phi k\} \\ + \frac{1}{2}\exp\{j2\pi(f_x^v + f_p^v) l T_{prf} - j\Phi k\} \end{aligned} \tag{3.5.8}$$

and

$$\begin{aligned} r_{sqh}(k,l) = \frac{1}{2j}\{\exp(j\Phi k - j2\pi f_p^v l T_{prf}) - \exp(j2\pi f_p^v l T_{prf} - j\Phi k)\} \\ \times \exp(j2\pi f_x^v l T_{prf}) = \frac{1}{2j}\exp\{j2\pi(f_x^v - f_p^v) l T_{prf} + j\Phi k\} \\ - \frac{1}{2j}\exp\{j2\pi(f_x^v + f_p^v) l T_{prf} - j\Phi k\} \end{aligned} \tag{3.5.9}$$

[2] Euler's formula: $sin(x) = \frac{e^{ix} - e^{-ix}}{2i}$ and $cos(x) = \frac{e^{ix} + e^{-ix}}{2}$

Using (3.5.8) and (3.5.9), two new signals r_1 and r_2 can be composed

$$r_1(k,l) = r_{sq}(k,l) + jr_{sqh}(k,l) = \exp\{j(2\pi(f_p^v + f_x^v)lT_{prf} + \Phi k)\} \tag{3.5.10}$$

$$r_2(k,l) = r_{sq}(k,l) - jr_{sqh}(k,l) = \exp\{j(2\pi(f_x^v - f_p^v)lT_{prf} - \Phi k)\} \tag{3.5.11}$$

The above mentioned signals has been used by Pamela Buratti in her master thesis [31] to estimate the spectrogram, but since she didn't have access to the realistic data, she was not able to test the method proposed in her master thesis on real data. There were two problems in her way of estimating the PSD. First, she didn't compensate for the axial velocity component in the generated data to estimate transversal velocity, which following will be done by multiplying the two signals. Second, she considered the phase shift factor according to the depth when using BIAA, which following will be canceled during the process of generating new signal. Then, to find the appropriate signal for estimation of transversal velocity, i.e., a signal without axial velocity component, r_1 and r_2 are multiplied and a new signal was generated.

$$r_{12}(k,l) = \exp\{j2\pi(2f_x^v)lT_{prf}\} \tag{3.5.12}$$

This new sinusoidal signal, $r_{12}(k,l)$, has a frequency $f_r = 2f_x^v = 2v_x/d_x$ and no contribution from axial velocity. This allows the lateral blood velocity to be estimated by using (3.5.12).

Chapter 4

POWER SPECTRAL ESTIMATION

As we have seen before, the problem of estimation of blood velocity reduces to estimating the power spectral density (PSD) of the received signal. Existing ultrasonic scanners mainly use a Welch-based spectral estimation technique to form an estimate of the blood velocity spectrum. However, these methods suffer from poor resolution and leakage problems [16]. Therefore, in recent works, there has been some interest in deriving other more robust spectral estimation techniques, allowing for better estimates. In this chapter, we will introduce Filterbank (FB) methods, and give a short introduction of the BIAA (Blood Iterative Adaptive Approach), which is one of FB methods derived to estimate blood velocities.

4.1 Filterbank Methods

Stocia and Moses review a large range of different spectral estimation techniques, forming an estimate of the PSD of a signal, $\{\phi(w)\}_{w=-\pi}^{\pi}$, from a finite number of samples [16]. One of these techniques that is of particular interest here is the so-called filterbank technique. This approach is formed by making the assumption that $\phi(w)$ is nearly constant over the interval $[w - \beta\pi, w + \beta\pi]$, for some given $\beta \ll 1$.
Figure 4.1 motivates the name of *filterbank methods*, The band-pass filter in this figure, which sweeps through the frequency interval of interest, can be viewed as a bank of (band-pass) filters. Depending on the band-pass filter chosen, we may obtain various filterbank methods of spectral estimation. Assuming that

1. $\phi(w)$ is nearly constant over the filter pass-band;
2. The filter gain is nearly one over the pass-band and zero outside the pass-band;
3. The power of the filtered signal is consistently estimated.

the PSD estimate $\widehat{\phi}_{FB}(w)$, obtained through the filterbank approach, is a good approximation of $\phi(w)$ [16]. As shown in [16], if all three above assumptions are

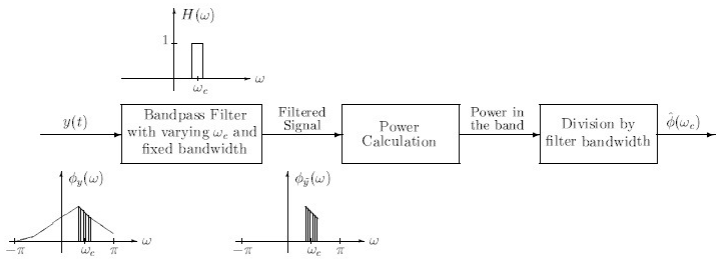

Figure 4.1. The filterbank approach to PSD estimation. Figure from [16].

satisfied, then a high resolution and low variance spectral estimates will be gained. In reality, this is not the case and there will as usual be a trade-off between resolution and statistical variability, and the resolution is limited by the sample length. Data-adaptive FB methods are a subset of filterbank methods that data properties are considered in the construction of filters, and since they do not make any assumption on model orders and perform excellently, and give higher resolution in compare to Welch methods, there is a significant interest in using them, specially when a high resolution is needed [32]. The cost for their advantages is more computational complexity. In [18], the authors have proposed an iterative blood velocity spectral estimators, which is called BIAA. In the following, this approach will be explained and some small changes have been made to use it for transversal blood velocity estimation.

4.2 Blood Iterative Adaptive Approach algorithm

The Blood Iterative Adaptive Approach (BIAA) was introduced in [18] and it will be reviewed here. The BIAA algorithm is an iterative and data adaptive methods for blood velocity estimation by using medical ultrasound scanners. One of its major properties is that there is no need to make any assumption on the sampling pattern (both in slow and fast time samples), so it allows for the duplex mode transmission which is necessary for B-mode images. Moreover, it still gives an accurate estimation even with a few number of samples, so makes it possible to estimate the blood velocity in two different regions of the vessel, while still there will be enough data to generate the B-mode image. And as was shown in [18], the BIAA technique outperforms the other data-adaptive techniques by presenting fewer spectral artifacts.

4.2.1 Theory and methods for axial BIAA

A detailed description of the BIAA algorithm for estimation of axial blood velocity which is given in [18] will be given here. The same notation is used here for data models and most of the text in this part is from [18]. Considering the sampled signal at depth k corresponding to emission n as

$$\mathbf{x}_k(n) = \alpha_{v_z} exp(j\phi k + j\psi_{v_z} n) + \mathbf{w}_k(n) \tag{4.2.1}$$

where α_{v_z} is the the (complex-valued) amplitude of the sinusoidal signal at frequency ψ_{v_z}, and is given by

$$\psi_{v_z} = -\frac{2\omega_c}{cf_{prf}} v_z = -\frac{2\omega_c}{c} v_z T_{prf} \tag{4.2.2}$$

where $\omega_c = 2\pi f_c$, and T_{prf} is the pulse repetitions time , Furthermore, ϕ is the demodulating frequency related to the sample's depth, and is defined as

$$\phi = \frac{\omega_c}{f_s}$$

where f_s is the sampling frequency, and $\mathbf{w}_k(n)$ denotes a residual term that contains signals at velocity different from v_z and also contains the noise. From (4.2.1) and (4.2.2), we see that the PSD with respect to ψ_{v_z} is equivalent to the blood velocity distribution at the same location, so by estimating $|\alpha_{v_z}|^2$ for each velocity of interest an estimation of blood velocity can be obtained. There is no need to make any assumption on sampling pattern over fast, nor slow time. The signal in (4.2.1) can be written as the sum of contributions from each frequency grid point $\{\psi_{m,v_z}\}_{m=1}^{M}$,

$$\mathbf{x}_k(n) = \exp(j\phi k) \sum_{m=1}^{M} \alpha_{m,v_z}^{(k)} \exp(j\psi_{m,v_z} n) + e_k(n) \tag{4.2.3}$$

where $e_k(n)$ is considered to be a zero mean white complex Gaussian noise with variance η; this means that any possible noise coloring is modeled by the first term in (4.2.3), i.e., the signal part. Since blood has a smooth flow profile, the amplitude of PSD at each depth will be almost constant over a range of depths, $\alpha_{m,v_z}^{(k)}$, $k = k_1, ..., k_K$. Moreover, since ϕ is known,

$$\mathbf{z}_k(n) = \exp(-j\phi k)\mathbf{x}_k(n)$$

is introduced and in a compact form

$$\mathbf{z}_k = \mathbf{A}\alpha_{v_z}^{(k)} + \mathbf{e}_k$$

where for $n = n_1, ..., n_N$

$$\mathbf{z}_k = [z_k(n_1) \ ... \ z_k(n_N)]^T$$

$$\alpha_{v_z}^{(k)} = [\alpha_{1,v_z}^{(k)} \ ... \ \alpha_{M,v_z}^{(k)}]^T$$

$$\mathbf{A} = [\mathbf{a_1} \ ... \ \mathbf{a_M}]$$

$$\mathbf{a_m} = [\exp(j\psi_{m,v_z} n_1) \ ... \ \exp(j\psi_{m,v_z} n_N)]^T$$

and where $\mathbf{e}_k$ is defined similarly to $\mathbf{z}_k$. Since blood profile is smooth, an estimate of the central amplitude can be found by averaging over the neighboring amplitude,

$$\hat{\alpha}_{m,v_z} = \frac{1}{K} \sum_{k=k_1}^{k_K} \hat{\alpha}_{m,v_z}^{(k)}$$

What is left is to find $\hat{\alpha}_{m,v_z}^{(k)}$, $m = 1, .., M$, which is done by using the BIAA algorithm.

4.2.2 Axial BIAA

To get a better understanding of algorithm, the steps of acquiring this algorithm, given in [18] will be explained here. It was shown that $|\hat{\alpha}_{m,v_z}^{(k)}|^2$ is a measure of the blood spectral density at velocity v_z. The covariance matrix of data z_k can be expressed as.

$$\mathbf{R_B}^{(k)} = \sum_{m=1}^{M} |\alpha_{m,v_z}^{(k)}|^2 \mathbf{a_m} \mathbf{a_m} * + \eta \mathbf{I_N} = \mathbf{A} \mathbf{P_B}^{(k)} \mathbf{A}^* + \eta \mathbf{I_N}, \tag{4.2.4}$$

where $\mathbf{P_B}^{(k)}$ is the power matrix defined as

$$\begin{aligned} \mathbf{P_B}^{(k)} &= diag\left(\left[p_B^{(1,k)} \cdots p_B^{(M,k)}\right]\right), \\ p_B^{(m,k)} &= |\alpha_{m,v_z}^{(k)}|^2. \end{aligned} \tag{4.2.5}$$

where $diag(\mathbf{v})$ represents the matrix that has the elements of the vector $\mathbf{v}$ along its diagonal. The covariance matrices can be averaged over different depths:

$$\mathbf{R_B} = \frac{1}{K} \sum_{k=k_1}^{k_K} \mathbf{R_B}^{(k)} = \frac{1}{K} \mathbf{A} \left[\sum_{k=k_1}^{k_K} P_B^{(k)} \right] \mathbf{A}^* + \eta \mathbf{I}. \tag{4.2.6}$$

Then the inference covariance matrix, i.e., that has the contribution from all points on the frequency grid except ψ_{m,v_z}, can be defined as

$$\mathbf{Q}_m = \mathbf{R_B} - |\alpha_{m,v_z}^{(k)}|^2 \mathbf{a_m} \mathbf{a}_m^* \tag{4.2.7}$$

General linear estimator is used to find the estimate of : $\hat{\alpha}_{m,v_z}^{(k)} = \mathbf{h}_m^* \mathbf{z}_k$ then the weight vector can be find by solving

$$\min_{h_m} h_m^* \widehat{Q_m}(\omega) h_m \qquad \text{subject to} \quad h_m^* \mathbf{a}_m = 1, \tag{4.2.8}$$

and the minimizer is found as

$$\widehat{h}_m = \frac{\mathbf{R}_B^{-1}\mathbf{a}_m}{\mathbf{a}_m^* \mathbf{R}_B^{-1}\mathbf{a}_m} \tag{4.2.9}$$

then an estimate of amplitude will be

$$\hat{\alpha}_{m,v_z}^{(k)} = \frac{\mathbf{a}_m^* \mathbf{R}_B^{-1}\mathbf{z}_k}{\mathbf{a}_m^* \mathbf{R}_B^{-1}\mathbf{a}_m} \tag{4.2.10}$$

So only the noise variance η, should be estimated. For each slow-time sample n and fast-time sample k

$$\widehat{\eta}_{n,k} = \left| \frac{\mathbf{v}_n^* \mathbf{R}_B^{-1}\mathbf{z}_k}{\mathbf{v}_n^* \mathbf{R}_B^{-1}\mathbf{v}_n} \right|^2, \tag{4.2.11}$$

where $\mathbf{v}_n$ is the nth column of $\mathbf{I}_N$. The noise variance estimate is then computed as

$$\widehat{\eta}_B = \frac{1}{NK} \sum_{n=n_1}^{n_N} \sum_{k=k_1}^{k_K} \widehat{\eta}_{n,k}. \tag{4.2.12}$$

As suggested in [18], a least square (LS) estimation can be used as initialization for amplitude

$$\hat{\alpha}_{m,v_z}^{(k)} = \mathbf{a}_m^* \mathbf{z}_k / N$$

and a small number, e.g., 10^{-9} as noise variance estimate. The BIAA spectral estimators are thus found by iterating the estimation of $\mathbf{R}_B$ in (4.2.6) and amplitude in (6.2.4) until a stopping criteria is satisfied, which generally will be satisfied after no more than 10-15 iterations [18]. An outline of this algorithm is shown in Table 4.1.

4.2.3 Theory and methods for transversal BIAA

Herein, the necessary steps to apply BIAA for estimation of transversal blood velocity will be described. In section 3.5 it was shown that the signal that contains the transversal velocity contribution can be written as

$$r(k,l) = \alpha_{v_x} \exp(j2\pi(2f_x^v) l T_{prf}) + \mathbf{w}(k,l) \tag{4.2.13}$$

Introducing $\psi_{v_x} = 2\pi(2f_x^v)T_{prf}$ and rewriting (4.2.13) as the sum of contributions from each frequency grid point $\{\psi_{m,v_x}\}_{m=1}^M$ gives us

$$r(k,l) = \sum_{m=1}^{M} \alpha_{v_x}^{(k)} \exp(j\psi_{m,v_x}) + e(k,l) \tag{4.2.14}$$

Table 4.1. Outline of the BIAA algorithm for axial velocity estimation

Initialize:	$\mathbf{z}_k(n) = \exp(-j\phi k)\mathbf{x}_k(n)$
	$\hat{\alpha}_{m,v_z}^{(k)} = \mathbf{a}_m^* \mathbf{z}_k / N$
	$\widehat{\eta} = 10^{-9}$
Step1	$p_B^{(m,k)} = \lvert\hat{\alpha}_{v_z,v_x}^{(m,k)}\rvert^2$
Step2	$\mathbf{P_B}^{(k)} = diag\left(\left[p_B^{(1,k)} \cdots p_B^{(M,k)}\right]\right)$
	$\mathbf{P_B} = \frac{1}{K}\sum_{k=k_1}^{k_K} \mathbf{P_B}^{(k)}$
	$\mathbf{R_B} = \frac{1}{K}\mathbf{A}\mathbf{P_B}^{(k)}\mathbf{A}^* + \hat{\eta}_B\mathbf{I}$
Step3	$\hat{\alpha}_{m,v_z}^{(k)} = \dfrac{\mathbf{a}_m^*\mathbf{R}_B^{-1}\mathbf{z}_k}{\mathbf{a}_m^*\mathbf{R}_B^{-1}\mathbf{a}_m}$
Step4	$\widehat{\eta}_{n,k} = \left\lvert\dfrac{\mathbf{v}_n^*\mathbf{R}_B^{-1}\mathbf{z}_k}{\mathbf{v}_n^*\mathbf{R}_B^{-1}\mathbf{v}_n}\right\rvert^2$
	$\widehat{\eta}_B = \frac{1}{NK}\sum_{n=n_1}^{n_N}\sum_{k=k_1}^{k_K} \widehat{\eta}_{n,k}$
Step5	repeat steps 1-4 until practical convergence
Finalize	$\hat{\alpha}_{m,v_z} = \frac{1}{K}\sum_{k=k_1}^{k_K} \hat{\alpha}_{m,v_z}^{(k)}$

where $e(k,l)$ is a zero mean white complex Gaussian noise with variance η; this means that any possible noise coloring is modeled by the first term in (4.2.14), i.e., the signal part. By introducing

$$\mathbf{r}_k = \mathbf{A}\alpha_{v_x}^{(k)} + \mathbf{e}_k$$

where

$$\mathbf{r}_k = [z_k(l_1) \ ... \ z_k(l_N)]^T$$
$$\alpha_{v_x}^{(k)} = [\alpha_{1,v_x}^{(k)} \ ... \ \alpha_{M,v_x}^{(k)}]^T$$
$$\mathbf{A} = [\mathbf{a_1} \ ... \ \mathbf{a_M}]$$

where

$$\mathbf{a_m} = [\exp(j\psi_{m,v_x} l_1) \ ... \ \exp(j\psi_{m,v_x} l_N)]^T$$

and where $\mathbf{e}_k$ is defined similarly to $\mathbf{z}_k$. From the estimate of the amplitude at depth k, $\hat{\alpha}^{(k)}_{m,v_x}$, due to the smoothness of the blood flow profile, the central amplitude can estimated be by simply averaging the neighboring amplitude estimates

$$\hat{\alpha}_{m,v_x} = \frac{1}{K} \sum_{k=k_1}^{k_K} \hat{\alpha}^{(k)}_{m,v_x}$$

It now remains to find $\hat{\alpha}^{(k)}_{m,v_x}$, $m = 1, .., M$, which is done by using BIAA algorithm for transversal velocity.

4.2.4 Transversal BIAA

An outline of BIAA algorithm for estimation of transversal blood velocity can be seen in Table 4.2.

Table 4.2. Outline of the BIAA algorithm for transversal velocity estimation

Initialize:	$\hat{\alpha}_{m,v_x}^{(k)} = \mathbf{a}_m^* \mathbf{r}_k / N$
	$\widehat{\eta} = 10^{-9}$
Step1	$p_B^{(m,k)} = \lvert\hat{\alpha}_{v_x}^{(m,k)}\rvert^2$
Step2	$\mathbf{P_B}^{(k)} = diag\left(\left[p_B^{(1,k)} \cdots p_B^{(M,k)}\right]\right)$
	$\mathbf{P_B} = \frac{1}{K} \sum_{k=k_1}^{k_K} \mathbf{P_B}^{(k)}$
	$\mathbf{R_B} = \frac{1}{K} \mathbf{A} \mathbf{P_B}^{(k)} \mathbf{A}^* + \hat{\eta}_B \mathbf{I}$
Step3	$\hat{\alpha}_{m,v_x}^{(k)} = \dfrac{\mathbf{a}_m^* \mathbf{R}_B^{-1} \mathbf{z}_k}{\mathbf{a}_m^* \mathbf{R}_B^{-1} \mathbf{a}_m}$
Step4	$\widehat{\eta}_{n,k} = \left\lvert \dfrac{\mathbf{v}_n^* \mathbf{R}_B^{-1} \mathbf{r}_k}{\mathbf{v}_n^* \mathbf{R}_B^{-1} \mathbf{v}_n} \right\rvert^2$
	$\widehat{\eta}_B = \frac{1}{NK} \sum_{n=n_1}^{n_N} \sum_{k=k_1}^{k_K} \widehat{\eta}_{n,k}$
Step5	repeat steps 1-4 until practical convergence
Finalize	$\hat{\alpha}_{m,v_x} = \frac{1}{K} \sum_{k=k_1}^{k_K} \hat{\alpha}_{m,v_x}^{(k)}$

Chapter 5

ANALYSIS OF THE PERFORMANCE

In this chapter, the performance of the BIAA algorithm to estimate both axial and transversal velocity is examined in a realistic situation, where the data was generated by using Field II toolbox [19]. The results are compared with those of the so-called second-order[1] and the fourth-order methods [30].

5.1 Femoral artery simulation

To compare the methods in a realistic scenario, the Field II program [19] was used to generate flow data, using the Womersley model [33] for pulsating flow from the femoral artery, where the exact result of the velocity estimation is known. Figure 5.1[2] shows the mean velocity profile of femoral artery with propagation angle $\theta = 60^0$. The specific parameters for the flow simulation are summarized in Table 5.1.

The stationary part of the signal was removed by subtraction of the mean of the signal, which is a common way to remove the signals from stationary echos. Moreover, all spectrograms were produced using a dynamic range of 30 dB. The velocity has been estimated in the center of vessel and 30 samples along depth were used to generate PSD. The number of emissions to generate one vertical line in spectrogram, and the angle of propagation has been varied and the result from the three different methods compared. To get better resolution, for the price of using an additional beamforming, axial velocity was calculated in conventional way and transversal velocity was generated by using two more beamformers, which are used to generate signals needed for estimation of transversal velocity.

[1] This method use a cross correlation approach to estimate velocities.
[2] This figure was generated by using the codes by Professor Jørgen Arendt Jensen.

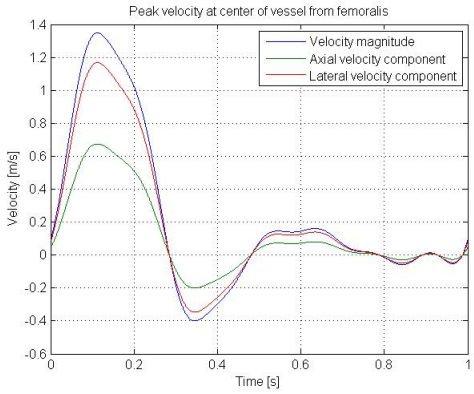

Figure 5.1. Mean velocity profile for femoral artery

Table 5.1. Parameters for transducer and femoral flow simulation

Transducer center frequency	f_0	3.42 MHz
Pulse cycles	M	8
Speed of sound	c	1540 m/s
Pitch of transducer element	w	0.33 mm
Height of transducer element	h_e	13 mm
Kerf	k_e	.0165 mm
Number of active elements	N_e	128
Corresponding range gate size		123 mm
Sampling frequency	f_s	25 MHz
Pulse repetition frequency	f_{prf}	15 kHz
Radius of vessel	R	4.2 mm
Distance to vessel center	Z_{ves}	40 mm
Angle between beam and flow		60^0

5.1.1 Number of emissions = 128

Figure 5.2 shows the estimated spectrogram, where 128 beams, the whole active elements, are used to estimate each line of PSD and spectrogram, and PSD was generated with 15 samples overlap. Subfigures in each row show the results from different propagation angles, i.e. $\theta = 90^0,\ 75^0$, and 60^0, respectively, and subfigures in first column (i.e., (a), (d), and (g)) show the results from BIAA, subfigures in second column (i.e., (b), (e), and (h)) show the results from second-order method and finally, subfigures in third column (i.e., (c), (f), and (i)) show the results from

the Fourth-order method. In each of subfigures, the lateral velocity estimation can be seen on top of axial velocity estimation with the known mean velocity profile being shown as the blue line.

It can be seen that BIAA has the best resolution with less artifacts in estimation of both transversal and axial spectrum. Now we proceed, by decreasing the number of emission necessary for generating a single line of PSD, and investigate the effect on each of the methods.

5.1.2 Number of emissions = 64

Figure 5.3 shows the same thing but this time 64 beams are emitted to estimate each spectrum line and 15 sample overlap was used. Again we can see better resolution with less artifacts from BIAA for estimation of both spectrum.

5.1.3 Number of emissions =32

Figure 5.4 shows the spectrogram where 32 beams are emitted to estimate each spectrum line. The spectrogram was generated with 15 samples overlap so half of the samples were reused for the creation of the each PSD line. Again we can see better results from BIAA for estimation of both spectrum.

5.1.4 Number of emissions =16

Figure 5.5 shows the same spectrogram, where this time 16 beams are emitted to estimate each spectrum line. The spectrogram was generated with 15 samples overlap so almost all of the samples except one were reused for the creation of each PSD line.

5.1.5 Number of emissions =8

Finally, Figure 5.6 shows the results for 8 emissions. The spectrogram was generated with 4 samples overlap. And we can see that BIAA still works well at estimation of axial spectrum but estimation of transversal spectrum becomes a little bit worse. However, it still works much better than two other methods and can keep track of velocity.

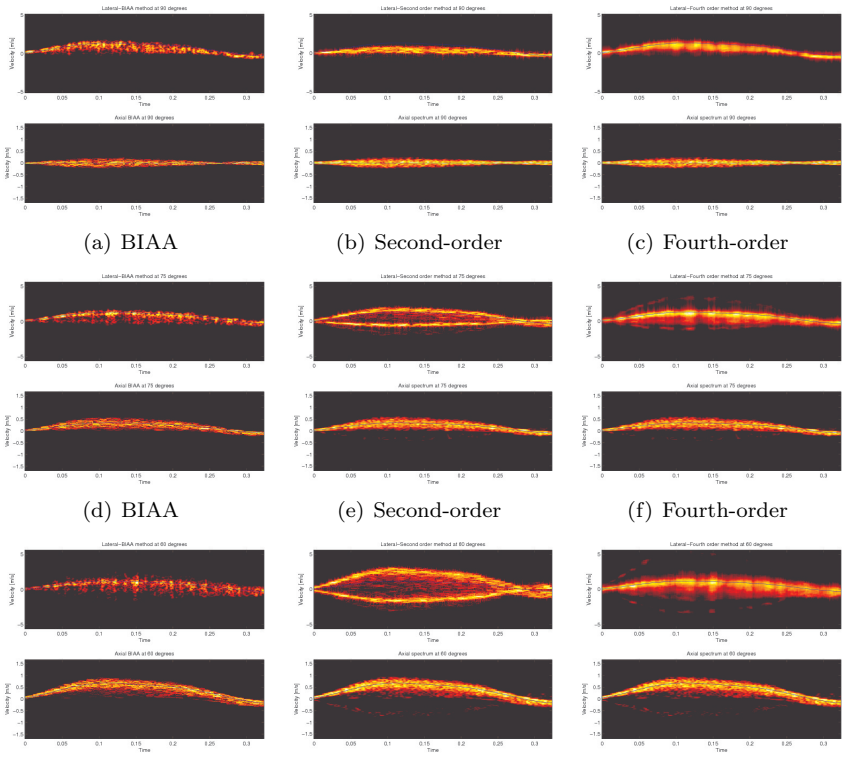

(a) BIAA (b) Second-order (c) Fourth-order

(d) BIAA (e) Second-order (f) Fourth-order

(g) BIAA (h) Second-order (i) Fourth-order

Figure 5.2. In each subfigure transversal blood velocity profile can be seen on top of axial velocity, which has been estimated by using the simulated data from femoral artery. ***128*** emissions to calculate each line of PSD was used. Figures in first, second and third row show the results from propagation angles $\theta = 90^0$, 75^0, and 60^0, respectively.

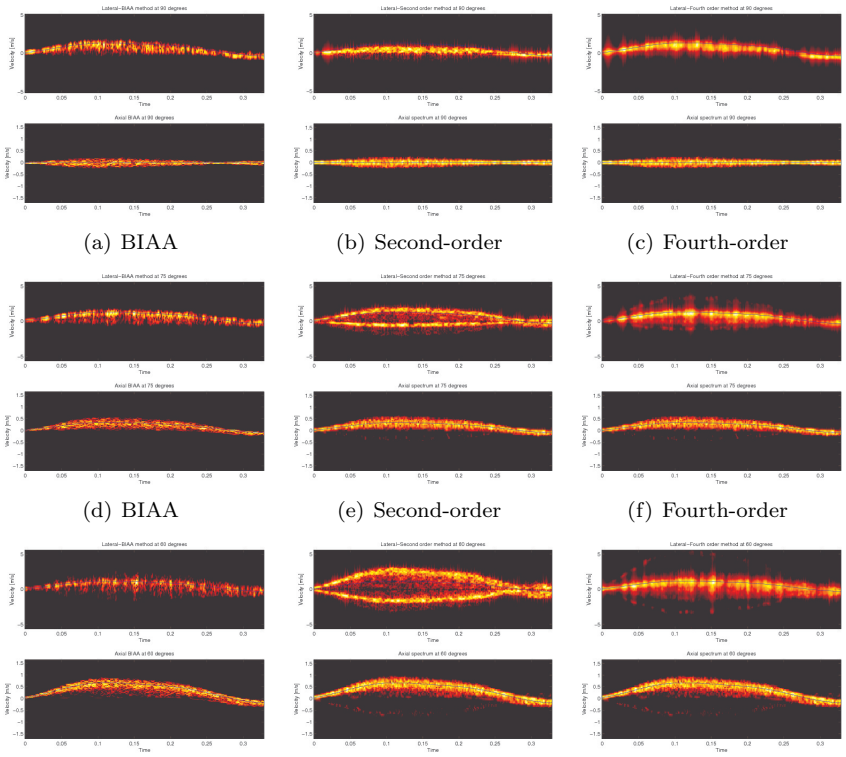

(a) BIAA (b) Second-order (c) Fourth-order

(d) BIAA (e) Second-order (f) Fourth-order

(g) BIAA (h) Second-order (i) Fourth-order

Figure 5.3. In each subfigure transversal blood velocity profile can be seen on top of axial velocity, which has been estimated by using the simulated data from femoral artery. ***64*** emissions to calculate each line of PSD was used. Figures in first, second and third row show the results from propagation angles $\theta = 90^0$, 75^0, and 60^0, respectively.

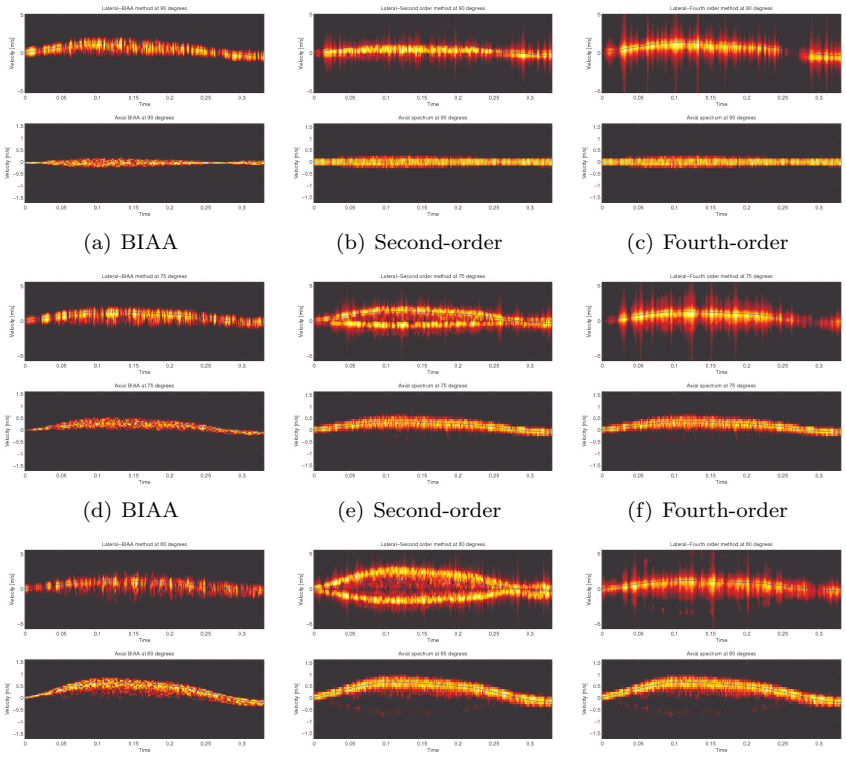

(a) BIAA (b) Second-order (c) Fourth-order

(d) BIAA (e) Second-order (f) Fourth-order

(g) BIAA (h) Second-order (i) Fourth-order

Figure 5.4. In each subfigure transversal blood velocity profile can be seen on top of axial velocity, which has been estimated by using the simulated data from femoral artery. ***32*** emissions to calculate each line of PSD was used. Figures in first, second and third row show the results from propagation angles $\theta = 90^0$, 75^0, and 60^0, respectively.

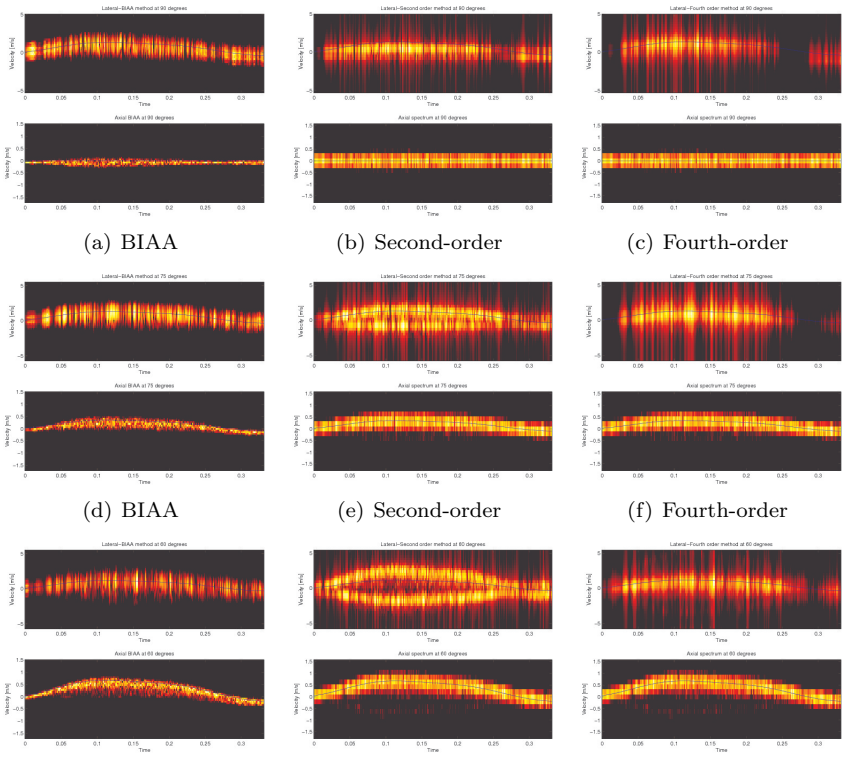

(a) BIAA (b) Second-order (c) Fourth-order

(d) BIAA (e) Second-order (f) Fourth-order

(g) BIAA (h) Second-order (i) Fourth-order

Figure 5.5. In each subfigure transversal blood velocity profile can be seen on top of axial velocity, which has been estimated by using the simulated data from femoral artery. ***16*** emissions to calculate each line of PSD was used. Figures in first, second and third row show the results from propagation angles $\theta = 90^0$, 75^0, and 60^0, respectively.

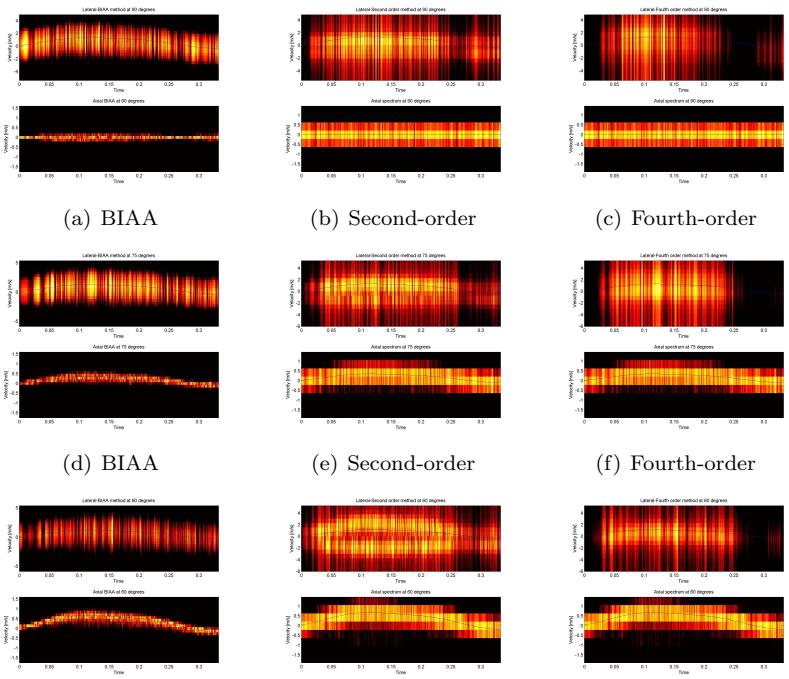

(a) BIAA (b) Second-order (c) Fourth-order

(d) BIAA (e) Second-order (f) Fourth-order

(g) BIAA (h) Second-order (i) Fourth-order

Figure 5.6. In each subfigure transversal blood velocity profile can be seen on top of axial velocity, which has been estimated by using the simulated data from femoral artery. ***8*** emissions to calculate each line of PSD was used. Figures in first, second and third row show the results from propagation angles $\theta = 90^0$, 75^0, and 60^0, respectively.

5.2 Conclusion

In this chapter, BIAA was used for estimation of both transversal and axial blood velocity, and it was seen that the BIAA algorithm provides spectrograms with fewer artifacts in comparison to other methods, moreover BIAA gives better results with less available samples which is so important for duplex mode transmissions, that a part of samples will be used to generate B-mode images. BIAA captures the transversal velocity pattern in situations that other methods cannot, and for axial velocity estimation it works perfectly well, even when a very small amount of samples are available. So it seems that it can be a good substitution to Welch-based methods in ultrasound systems that estimate both axial and transversal velocities.

Chapter 6

CLUTTER SUPRESSION

The backscattered signals from red blood cells, contain the clutter originating from stationary tissues in addition to the desired flow signal. The clutter's strength is typically 40 to 60 dB larger than the desired flow signal [34], so if they are not rejected efficiently, low velocity blood flow can not be measured, estimation of higher velocities will have a large bias [35]. Thus, it is important to remove the clutter to achieve an accurate velocity estimation, specially for in conditions like tumor imaging, that slow-flow is important in diagnose, where the blood and clutter often share the same Doppler frequency bands [34].

Different kinds of clutter filters, such as finite impulse response (FIR), infinite impulse response (IIR), and regression filter have been proposed to suppress the clutter from the backscattered signals ([36, 37], [35, 38] [39, 40]).

However, neither of these methods resulted in a better estimation of blood velocity, since clutter characteristics in color flow images vary. This might be a result of the nonstationary tissue motions which could be caused by a variety of factors, such as cardiac activities, respiration, transducer/patient movement [41], or a combination of them [34].

In the following, two novel methods to suppress the clutter will be explained. In both of these methods a secondary training data (STD) set, which only contains clutter plus noise signal, is used to get the necessary information to suppress clutter. The methods are evaluated on in vivo data, i.e., the data from examination of carotid artery[1] of a healthy volunteer by using the experimental scanner RASMUS [22]and a B-K Medical 8804, 7 MHz linear array transducer. This data set was previously used in [42].

6.1 Secondary training data (STD) set

Secondary training data is data without the signal of interest (SOI) that contains information about the interference. The interference cancellation method available today in other fields, e.g. SEAQUER [43] in Nuclear quadrupole resonance (NQR) application and adaptive clutter suppression methods based on iterative adaptive

[1] Carotid arteries are arteries that supply the head and neck with oxygenated blood.

approach in airborne radar application [20], project a signal onto the null space of the interference, receive the backscattered signal, and then remove it from the measurement [21]. Therefore, in blood velocity estimation, the first issue to deal with would be, how to get this data set. In this section low pass filtering of backscattered signal from blood vessel (which contains both SOI plus clutter and noise) is used to get a signal which only contains the data from clutter plus noise, and then this data will be used in the next sections to suppress the clutter.

6.1.1 Data model and methodology

Here, the backscattered signal from blood vessels which contains the signal of interest (SOI), the interference and the unstructured noise, is denoted as

$$z_k(n) = s_k(n) + r_k(n) + e_k(n) \tag{6.1.1}$$

where k and n are fast time and slow time indexes, respectively, $z_k(n)$ is the SOI at the same depth and time, $r_k(n)$ is the inference and $e_k(n)$ is the unstructured noise, often assumed to be Gaussian. The secondary training data set at the same fast and slow time denoted by $y_k(n)$ is made by only inference and noise.

$$y_k(n) = r_k(n) + \epsilon_k(n). \tag{6.1.2}$$

Since the the frequency of blood cells is much higher than clutter in some time intervals and therefore are not interleaved with clutter, the STD set can be obtained by low pass filtering of backscattered signal at those intervals. Then, this data can be used as a secondary training data set for clutter suppression.

6.1.2 Performance and result

To evaluate the method we use the in-vivo data from carotid artery of a healthy volunteer, gathered by using the experimental scanner RASMUS [22] and a B-K Medical 8804, 7 MHz linear array transducer. Figure 6.1 shows the spectogram of blood velocity by using BIAA algorithm on this data set. Table 6.1 shows the parameters for this calculation.

Here, to get a better understanding of impact of clutter the mean of the data was not removed (which is the conventional way of removing the clutter). Very powerful frequency components can be seen close to zero. Figure 6.2(a) shows the same spectrogram, but the frequency is shown on y-axis instead of velocity. As it can be seen from the figure most of the time, e.g. in the point shown by a blue arrow, the blood frequency and clutter frequency are so close to each other that cannot be separated but in some points, shown by green arrow, the blood frequency is much higher than the stationary echos. To get a better understanding, the PSD at these specific time points are shown in Figures 6.2(b) and 6.2(c).
The DSP system toolbox in Matlab was used to generate a low pass filter and this filter was applied on the time intervals where the blood velocity has much higher frequency component than inferences. Figure 6.3 shows one of these time intervals.

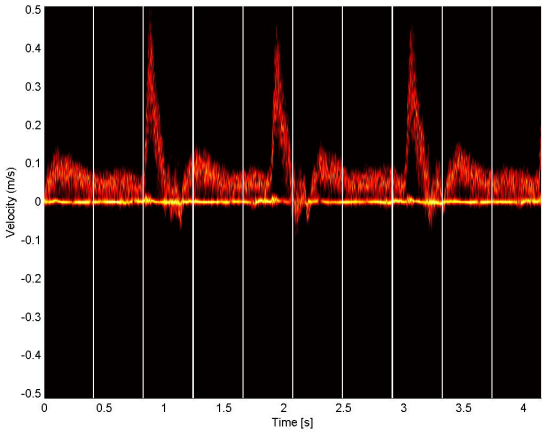

Figure 6.1. Spectrogram of blood velocity from carotid artery of a healthy volunteer.

Table 6.1. Parameters for Transducer and BIAA algorithm to estimate spectrogram of in-vivo data from carotid artery.

Transducer center frequency	f_0	7 MHz
Speed of sound	c	1540 m/s
Number of emissions for each PSD	N_e	32
Sampling frequency	f_s	40 MHz
Pulse repetition frequency	f_{prf}	9.3 kHz
Number of depth to average over in BIAA	N_d	40
Number of grid points in BIAA		1024
Maximum iteration of BIAA		15

Figure 6.4 shows the frequency response of the low pass filter which was used to generate the STD set and Table 6.2 shows it's properties.
To see how this filter work on the data, the filter was used on the whole data set and the spectrogram of filtered data was calculated. As it can be seen in Figure 6.5 the filter worked perfectly well on this data set, since the spectrogram only contains backscattered signal from clutter.

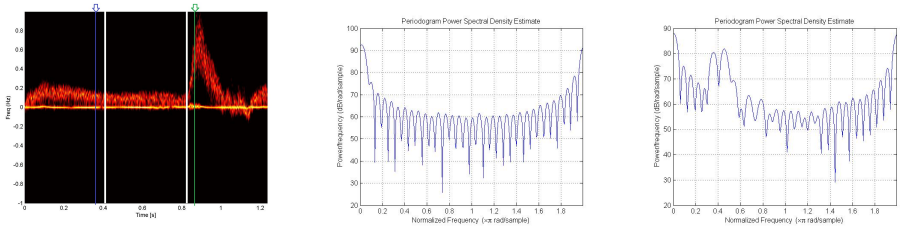

(a) Spectogram (b) PSD (c) PSD

Figure 6.2. Subfigure(a) Shows the spectrogram of blood velocity from carotid artery of a healthy volunteer. Subfigure(b) shows the PSD at a special point of slow time which is shown by a blue vertical line in subfigure(a). Subfigure(c) shows the PSD at green vertical line in subfigure(a)

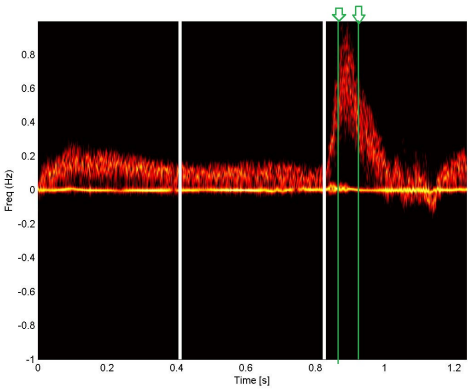

Figure 6.3. Section of data that after low pass filtering can be used as STD.

6.2 Adaptive Clutter Suppression Based on Iterative Adaptive Approach

In this part a new approach to improve the weighted-least-squares-based IAA, by using the secondary training data (STD) set is proposed. The idea was proposed in [20] to suppress clutter in airborne radar application. The aim of this method is to first use recently developed IAA to find the covariance matrix of the clutter plus noise (target absence) data set (STD set), then the resulting covariance matrix is applied to form a filter to suppress the clutter. Following, the same approach was examined to suppress the stationary echos effects from vessel's wall and surrounding tissues.

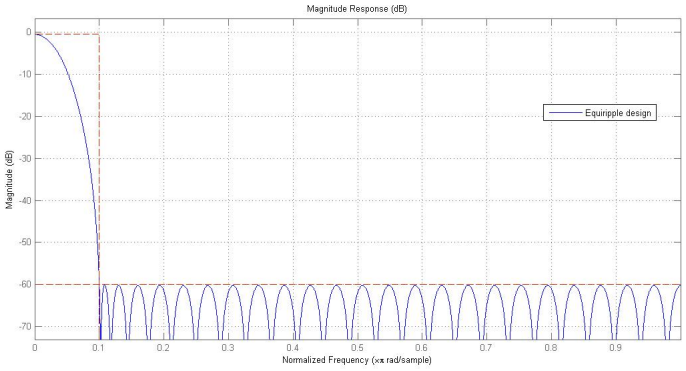

Figure 6.4. Frequency response of low pass filter used to generate STD.

Table 6.2. Low pass filter

Cutoff	$[0, 0.1]$
Passband ripple	1 dB
Stopband attenuation	60 dB
Order	Minimum order (49)
Method	Equiripple

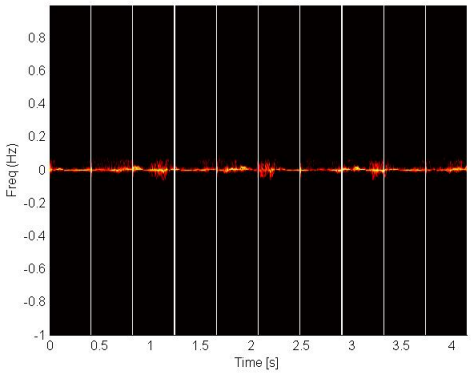

Figure 6.5. Spectrogram of low-pass filtered data with cut-off $[0, 0.1]$.

6.2.1 Data model and methodology

Considering the backscattered signal from emission number n at depth k as

$$z_k(n) = \alpha_v \exp(j\psi_v n) + e_k(n) \tag{6.2.1}$$

and writing it as a sum of contributions from each frequency grid point $\{\psi_{m,v}\}_{m=1}^{M}$:

$$z_k(n) = \sum_{m=1}^{M} \alpha_{m,v}^{(k)} \exp(j\psi_{m,v} n) + e_k(n) \tag{6.2.2}$$

or in a more compact form

$$\mathbf{z}_k = \mathbf{A}\alpha_v^{(k)} + \mathbf{w}_k \tag{6.2.3}$$

where

$$\mathbf{z}_k = [z_k(n_1) \ ... \ z_k(n_N)]^T$$

$$\alpha_v^{(k)} = [\alpha_{1,v}^{(k)} \ ... \ \alpha_{M,v}^{(k)}]^T$$

$$\mathbf{A} = [\mathbf{a_1} \ ... \ \mathbf{a_M}]$$

$$\mathbf{a_m} = [\exp(j\psi_{m,v} n_1) \ ... \ \exp(j\psi_{m,v} n_N)]^T$$

and where $\mathbf{w}_k$ is considered to be a zero mean white complex Gaussian noise with variance η and is defined similarly to $\mathbf{z}_k$. An estimate of amplitude at a given depth k and grid point m can be found as

$$\hat{\alpha}_{m,v}^{(k)} = \frac{\mathbf{a}_m^* \mathbf{R}_{IAA}^{-1} \mathbf{z}_k}{\mathbf{a}_m^* \mathbf{R}_{IAA}^{-1} \mathbf{a}_m} \tag{6.2.4}$$

where $\mathbf{R}_{IAA}$ is defined as (4.2.4).

The problem of conventional IAA is that it considers the signals reflected from stationary echoes, i.e., the signals coming from vessel boundaries and tissues around them are considered as a part of signal. In [20], Yang et al. proposed a new schema based on maximum likelihood estimation of covariance matrix of STD, R_{ML} and then using this estimation on IAA algorithm to adaptively finding the R_{IAA}. Table 6.3 shows the outline of their method, here called MIAA. In this table, $x_l, l = 1, 2, ..., L$ is L snapshot in STD which is assumed to have a complex multivariate IID Gaussian distribution with mean zero and covariance matrix $\mathbf{R}_{IAA}$, $\mathbf{X} = [x_1, ..., x_L]$, $a_{m,v}^{(k)} = |\hat{\alpha}_{m,v}^{(k)}|^2$ and where $\mathbf{v}_n$ is the nth column of $\mathbf{I}_N$.

Table 6.3. Outline of MIAA algorithm

Initialize:	$\hat{a}_{m,v}^{(k)} = \lvert\frac{\mathbf{a}_m^*\mathbf{x}}{\mathbf{a}_m^*\mathbf{a}_m}\rvert^2$ $\hat{\mathbf{R}}_{ML} = \frac{1}{L}\mathbf{X}\mathbf{X}^*$
step1	$\mathbf{R_{IAA}} = \sum_{m=1}^{M} \hat{a}_{m,v}^{(k)} a_m a_m^* + \widehat{\eta}_{IAA}\mathbf{I}$
step2	$\hat{a}_{m,v}^{(k)} = \frac{\mathbf{a}_m^*\mathbf{R}_{IAA}^{-1}\hat{\mathbf{R}}_{ML}\mathbf{R}_{IAA}^{-1}\mathbf{a}_m}{\left(\mathbf{a}_m^*\mathbf{R}_{IAA}^{-1}\mathbf{a_m}\right)^2}$
step3	$\widehat{\eta}_{n,k} = \left\lvert\frac{\mathbf{v}_n^*\mathbf{R}_{IAA}^{-1}\mathbf{x}}{\mathbf{v}_n^*\mathbf{R}_{B.}^{-1}\mathbf{v}_n}\right\rvert^2$ $\widehat{\eta}_{IAA} = \frac{1}{N}\sum_{n=n_1}^{n_N} \widehat{\eta}_{n,k}$
step4	repeat steps 1-3 until practical convergence

After obtaining clutter plus noise covariance matrix, the idea behind their method is to minimize the clutter plus noise output power whilst constraining the gain in direction of desired signal, which leads to the following minimization:

$$\min_{h_m} h_m^* \widehat{\mathbf{R}}_{IAA}(\omega) h_m \qquad \text{subject to} \quad h_m^* \mathbf{s}_m = 1, \tag{6.2.5}$$

where s_m is defined similar to a_m. This optimal filter is given by

$$\widehat{h}_m = \frac{\mathbf{R}_{IAA}^{-1}\mathbf{s}_m}{\mathbf{s}_m^*\mathbf{R}_{IAA}^{-1}\mathbf{s}_m} \tag{6.2.6}$$

then the target can be detected by the adaptive matched filter (AMF) detector with the form

$$\frac{\lvert\mathbf{s}_m^*\mathbf{R}_{IAA}^{-1}z_k\rvert^2}{\mathbf{s}_m^*\mathbf{R}_{IAA}^{-1}\mathbf{s}_m} \tag{6.2.7}$$

where z_k is the snapshot in the test range bin and if this detector is larger than a threshold it means that it comes from blood cells not wall of vessel.

6.2.2 Performance and result

To estimate the performance of this algorithm, the backscattred signal from examination of carotid artery was used as target presence data, and the data attained after low-pass filtering of this data in the time interval shown by Figure 6.3 was used as secondary data. The number of the emission which was used for each spectral line was 32, and the signal from the center of the vessel was examined, and the number of frequency grid points was 512. Figure 6.6 shows the result.

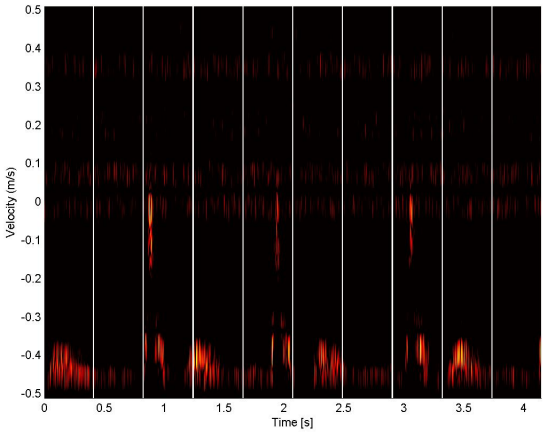

Figure 6.6. Spectrogram of blood velocity after suppression of clutter by using an Iterative Adaptive Approach

The result is strange. Therefore, to see how the method works on a single line of spectrum, the data from one line of spectrum, shown by a green line in Figure 6.7 was used and the method was applied on this data. The result can be seen in Figure 6.8, the left figure shows the PSD of the signal before using the method. The powerful clutter can be seen around zero, the figure in middle shows the PSD of STD, and the right figure shows the PSD of signal after suppression of clutter. As it can be seen, the method performs perfectly well on this segment of data.

So to see what cause the problem, the method was applied on a simple sinusoidal model, where some inferences around zero frequency were added to the signal, also some random noise. Figures 6.9 and 6.10 show the result of applying the method on this signal. As it can be seen in Figure 6.9, the clutter was suppressed perfectly well whereas in Figure 6.10 it was not. As the only difference between these two cases was the additive noise (because the noise was totally random), it means that the characteristic of noise can affect the performance of this algorithm.

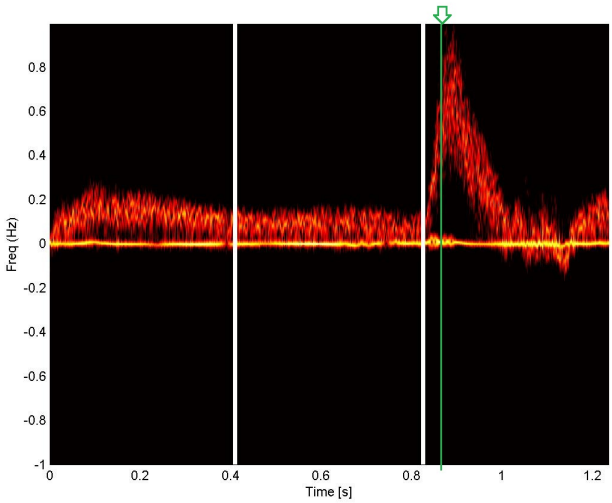

Figure 6.7. Spectral line which is used to examine impact of adaptive clutter suppression on blood velocity data

6.3 Inference cancellation by using STD

Next we examine a method proposed in [21] which named EPAIC (Estimation of Phase and Amplitude for Interference Cancellation), is suitable for all situations where measurements are contaminated by narrow-banded interference and where it is possible to collect secondary data. Considering the model described in (6.1.1) for SOI + clutter + noise (here called primary data), $z_k(n)$, and (6.1.2) for clutter + noise (here called secondary data), $y_k(n)$, it is considered that the narrow-banded stationary interference can be modeled as

$$r_k(n) = \sum_{k=1}^{K} \alpha_k \exp(2\pi j f_k n) \tag{6.3.1}$$

where α_k, and f_k are the complex amplitude, including the phase, and the frequency of k:th sinusoidal component in the interference respectively. K is assumed to be unknown. The main idea is to estimate the sinusoidal components in the interference and removing them from the primary data. The steps of the EPIAC algorithm [21], are given in Table 6.4.
The stopping criteria was chosen to be when an additional subtraction of a sinusoidal inference provide no more changes in secondary data.

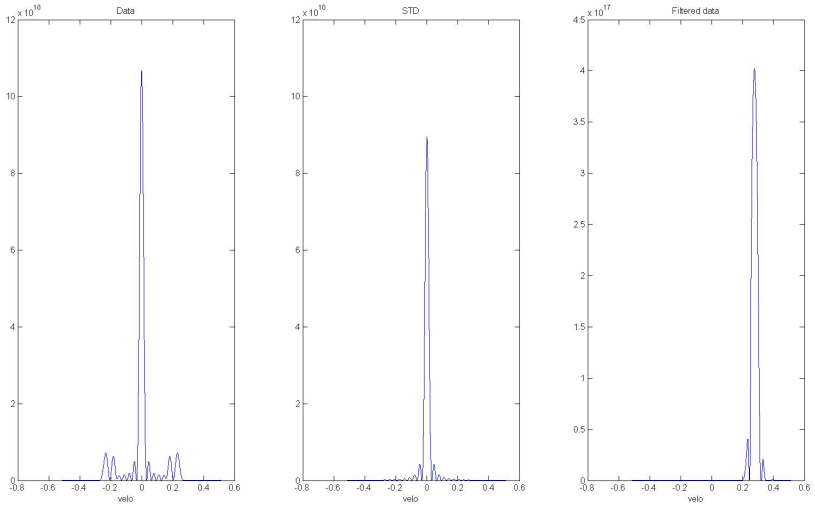

Figure 6.8. Power spectral of blood velocity after supression of clutter by using an Iterative Adaptive Approach for one line of spectrum.

Table 6.4. Algorithm EPIAC

1:	Given $z_k(n)$ and $y_k(n)$
2:	**while** Stopping criteria **do**
3:	Estimate the most dominant sinusoidal component in $r_k(n)$
4:	Remove it from $z_k(n)$
5:	Remove it from $y_k(n)$
6:	**end while**

6.3.1 Performance and result

Again low pass filtering of the backscattered signal from blood was used, as in section 6.1.2, to generate STD for blood velocity estimation, properties of used filter was the same as this section. The PSD of this data set can be seen in Figure 6.11. EPIAC was used on the two data set to remove the inference components from backscattered signal which again was gathered by examination of carotid artery of a healthy volunteer. The result for just one single line of spectrum, shown by a green line in Figure 6.7, can be seen in Figure 6.12.

It can be seen from figure that EPIAC works well in some parts, like interval shown between two green line in Figure 6.12, but it does not work for other parts that much good. It is somehow what can be expected from signals from blood.

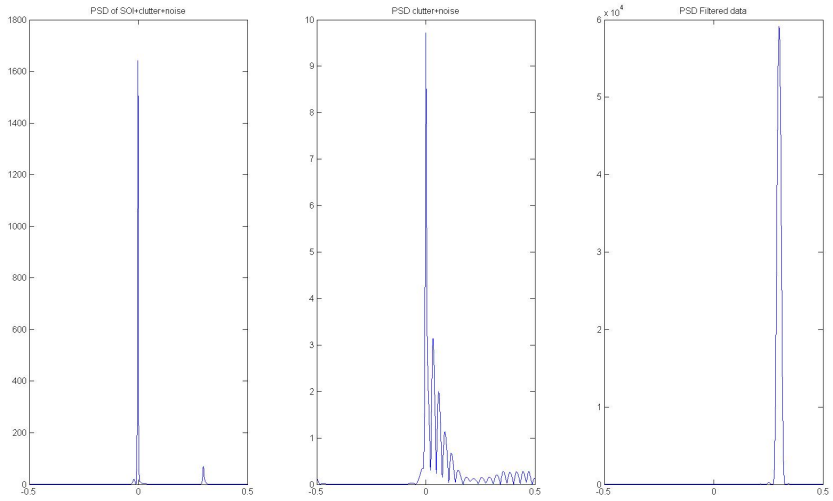

Figure 6.9. Power spectral of simple sinusoidal signal.

Since vessel's wall have nonstationary motions and this motion change according to pressure of blood flow. So they cannot be assumed to stationary in the whole cycle cycle.

6.4 Conclusion

In this chapter, two different methods have been examined to suppress the signals coming from stationary echos. However, neither of these methods resulted in a better estimation of blood velocity, since clutter characteristics in color flow images vary during time, which might be a result of the nonstationary tissue motions which could be caused by a variety of factors, such as cardiac activities, respiration, transducer/patient movement [41], and in both of these methods it was supposed that they are stationary. So a static filter cannot remove the clutter effectively. Moreover, it was shown that characteristic of the noise in blood velocity estimation may vary, which was one of the reasons that first method did not work on signals from blood. So the first method (6.2) does not seem to work on flow data and the second one (6.3) seems to works on short intervals but not for the whole blood flow cycle.

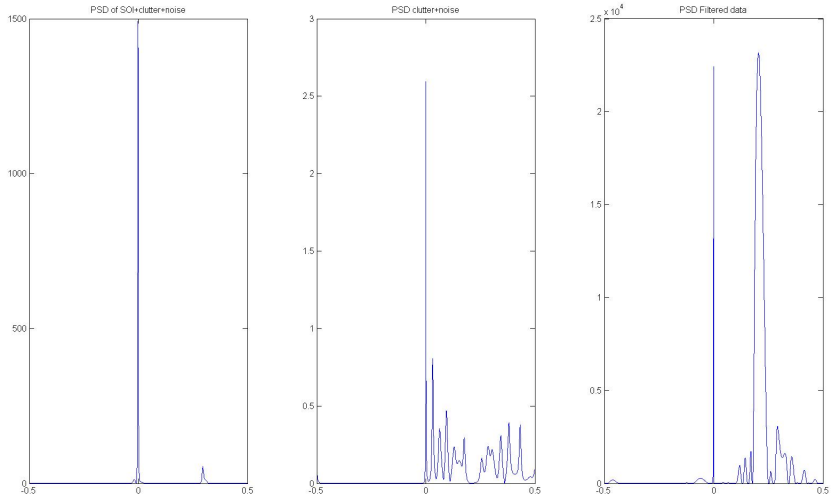

Figure 6.10. Power spectral of simple sinusoidal signal.

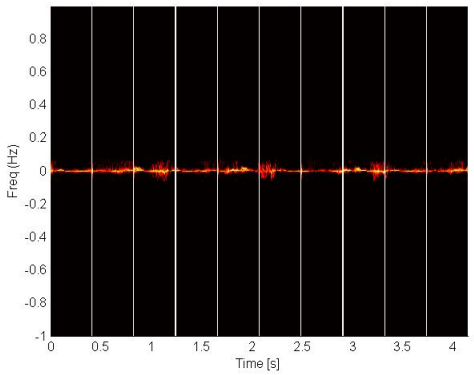

Figure 6.11. Spectrogram of low-pass filtered data with cut-off $[0, 0.1]$.

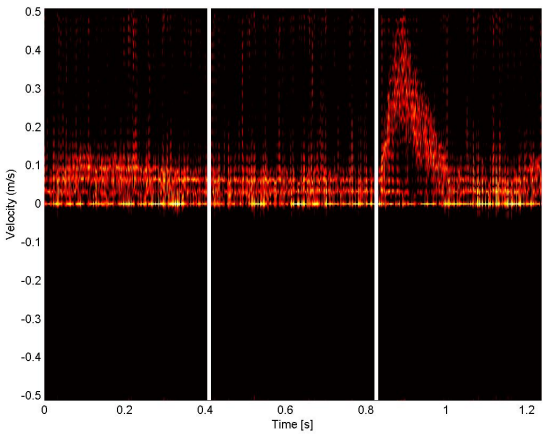

Figure 6.12. Blood velocity estimation after removing the clutter by using EPIAC

BIBLIOGRAPHY

[1] K. L. Hansen, "In-vivo studies of new vector velocity and adaptive spectral estimators in medical ultrasound.," *Danish medical bulletin*, vol. 57, no. 5, pp. 1–23, 2010.

[2] J. A. Jensen, *Estimation of Blood Velocities Using Ultrasound*. New York: Cambridge University Press, 1996.

[3] M. D. Fox, "Multiple crossed-beam ultrasound doppler velocimetry," *Sonics and Ultrasonics, IEEE Transactions on*, vol. 25, no. 5, pp. 281–286, 1978.

[4] G. E. Trahey, J. W. Allison, and O. T. van Ramm, "Angle independent ultrasonic detection of blood flow," vol. 34, pp. 965–967, 1987.

[5] V. L. Newhouse, D. Censor, T. Vontz, J. A. Cisneros, and B. B. Goldberg, "Ultrasound Doppler probing of flows transverse with respect to beam axis," vol. 34, pp. 779–788, 1987.

[6] O. Bonnefous, "Measurement of the complete (3d) velocity vector of blood flows," in *Ultrasonics Symposium, 1988. Proceedings., IEEE 1988*, pp. 795–799, IEEE, 1988.

[7] J. A. Jensen, "Directional velocity estimation using focusing along the flow direction. i: Theory and simulation," *Ultrasonics, Ferroelectrics and Frequency Control, IEEE Transactions on*, vol. 50, no. 7, pp. 857–872, 2003.

[8] J. A. Jensen and P. Munk, "A new method for estimation of velocity vectors," vol. 45, pp. 837–851, May 1998.

[9] J. A. Jensen, "A new estimator for vector velocity estimation," vol. 48, no. 4, pp. 886–894, 2001.

[10] M. E. Anderson, "Spatial quadrature: a novel technique for multi-dimensional velocity estimation," in *Ultrasonics Symposium, 1997. Proceedings., 1997 IEEE*, vol. 2, pp. 1233–1238, IEEE, 1997.

[11] M. Anderson, "A heterodyning demodulation technique for spatial quadrature," in *Ultrasonics Symposium, 2000 IEEE*, vol. 2, pp. 1487–1490, IEEE, 2000.

[12] J. Udesen and J. A. Jensen, "Investigation of transverse oscillation method," vol. 53, pp. 959 –971, may 2006.

[13] K. L. Hansen, J. Udesen, N. Oddershede, L. Henze, C. Thomsen, J. A. Jensen, and M. B. Nielsen, "In vivo comparison of three ultrasound vector velocity techniques to mr phase contrast angiography," *Ultrasonics*, vol. 49, no. 8, pp. 659–667, 2009.

[14] K. Hansen, J. Udesen, C. Thomsen, J. A. Jensen, and M. Nielsen, "In vivo validation of a blood vector velocity estimator with mr angiography," *Ultrasonics, Ferroelectrics and Frequency Control, IEEE Transactions on*, vol. 56, no. 1, pp. 91–100, 2009.

[15] M. M. Pedersen, M. J. Pihl, P. Haugaard, J. M. Hansen, K. L. Hansen, M. B. Nielsen, and J. A. Jensen, "Comparison of real-time in vivo spectral and vector velocity estimation.," *Ultrasound Med Biol*, vol. 38, pp. 145–51, 2012.

[16] P. Stoica and R. Moses, *Introduction to Spectral Analysis*. Upper Saddle River, N.J.: Prentice Hall, 1997.

[17] W. R. Hedrick, D. L. Hykes, and D. E. Starchman, *Ultrasound physics and instrumentation*. Mosby St. Louis, 1995.

[18] E. Gudmundson, A. Jakobsson, J. A. Jensen, and P. Stoica, "Blood Velocity Estimation Using Ultrasound and Spectral Iterative Adaptive Approaches," *Signal Process.*, vol. 91, pp. 1275–1283, May 2011.

[19] J. A. Jensen and N. B. Svendsen, "Calculation of pressure fields from arbitrarily shaped, apodized, and excited ultrasound transducers," vol. 39, pp. 262–267, 1992.

[20] Z. Yang, X. Li, H. Wang, and W. Jiang, "Adaptive Clutter Suppression Based on Iterative Adaptive Approach For Airborne Radar," *Elsevier Signal Processing*, vol. 93, pp. 3567–3577, 2013.

[21] J. Swärd and A. Jakobsson, "Interference Cancellation Using Secondary Data," in *39th International Conference on Acoustics, Speech, and Signal Processing*, 2014. Submitted.

[22] J. A. Jensen, O. Holm, L. J. Jerisen, H. Bendsen, S. I. Nikolov, B. G. Tomov, P. Munk, M. Hansen, K. Salomonsen, J. Hansen, K. Gormsen, H. M. Pedersen, and K. L. Gammelmark, "Ultrasound research scanner for real-time synthetic aperture data acquisition," vol. 52, pp. 881–891, May 2005.

[23] P. Munk, *Estimation of Blood Velocity Vectors using Ultrasound*. PhD thesis, DTU, 2000.

[24] A. C. Guyton, "Textbook of medical physiology," *The American Journal of the Medical Sciences*, vol. 242, no. 2, p. 136, 1961.

[25] M. J. Pihl, *3D vector flow imaging*. PhD thesis, DTU Electrical Engineering, 2012.

[26] C. Kasai, K. Namekawa, A. Koyano, and R. Omoto, "Real-time two-dimensional blood flow imaging using an autocorrelation technique," *IEEE Trans. Sonics Ultrason*, vol. 32, no. 3, pp. 458–464, 1985.

[27] D. Dotti, E. Gatti, V. Svelto, A. Ugge, and P. Vidali, "Blood flow measurements by ultrasound correlation techniques," *Energia Nucleare*, vol. 23, no. 11, pp. 571–575, 1976.

[28] O. Bonnefous and P. Pesque, "Time domain formulation of pulse-doppler ultrasound and blood velocity estimation by cross correlation," *Ultrasonic Imaging*, vol. 8, no. 2, pp. 73–85, 1986.

[29] S. G. Foster, P. M. Embree, and W. O'Brien Jr, "Flow velocity profile via time-domain correlation: Error analysis and computer simulation," *Ultrasonics, Ferroelectrics and Frequency Control, IEEE Transactions on*, vol. 37, no. 3, pp. 164–175, 1990.

[30] J. A. Jensen and P. Munk, "An improved estimation and focusing scheme for vector velocity estimation," in *Ultrasonics Symposium, 1999. Proceedings. 1999 IEEE*, vol. 2, pp. 1465–1470, IEEE, 1999.

[31] P. Buratti, "Eetimating blood velocity using ultrasound, new estimation techniques for axial and transversal velocities," Master's thesis, Department of Mathematical Statistics, Lund University, May 2010.

[32] T. Yardibi, J. Li, P. Stoica, M. Xue, and A. B. Baggeroer, "Source localization and sensing: A nonparametric iterative adaptive approach based on weighted least squares," *Aerospace and Electronic Systems, IEEE Transactions on*, vol. 46, no. 1, pp. 425–443, 2010.

[33] J. R. Womersley, "Oscillatory motion of a viscous liquid in a thin-walled elastic tube. I: The linear approximation for long waves," *Phil. Mag.*, vol. 46, pp. 199–221, 1955.

[34] Y. M. Yoo, R. Managuli, and Y. Kim, "Adaptive clutter filtering for ultrasound color flow imaging," *Ultrasound in medicine & biology*, vol. 29, no. 9, pp. 1311–1320, 2003.

[35] S. Bjaerum, H. Torp, and K. Kristoffersen, "Clutter filter design for ultrasound color flow imaging," *Ultrasonics, Ferroelectrics and Frequency Control, IEEE Transactions on*, vol. 49, no. 2, pp. 204–216, 2002.

[36] E. S. Chornoboy, "Initialization for improved iir filter performance," *Signal Processing, IEEE Transactions on*, vol. 40, no. 3, pp. 543–550, 1992.

[37] R. Peterson, L. Atlas, and K. Beach, "A comparison of iir initialization techniques for improved color doppler wall filter performance," in *Ultrasonics Symposium, 1994. Proceedings., 1994 IEEE*, vol. 3, pp. 1705–1708, IEEE, 1994.

[38] M. Shariati, J. Dripps, and W. McDicken, "Deadbeat iir based mti filtering for color flow imaging systems," in *Ultrasonics Symposium, 1993. Proceedings., IEEE 1993*, pp. 1059–1063, IEEE, 1993.

[39] A. Hoeks, J. Van de Vorst, A. Dabekaussen, P. Brands, and R. Reneman, "An efficient algorithm to remove low frequency doppler signals in digital doppler systems," *Ultrasonic imaging*, vol. 13, no. 2, pp. 135–144, 1991.

[40] A. P. Kadi and T. Loupas, "On the performance of regression and step-initialized iir clutter filters for color doppler systems in diagnostic medical ultrasound," *Ultrasonics, Ferroelectrics and Frequency Control, IEEE Transactions on*, vol. 42, no. 5, pp. 927–937, 1995.

[41] L. Thomas and A. Hall, "An improved wall filter for flow imaging of low velocity flow," in *Ultrasonics Symposium, 1994. Proceedings., 1994 IEEE*, vol. 3, pp. 1701–1704, IEEE, 1994.

[42] K. L. Hansen, F. Gran, M. M. Pedersen, I. K. Holfort, J. A. Jensen, and M. B. Nielsen, "In-vivo validation of fast spectral velocity estimation techniques," *Ultrasonics*, vol. 50, no. 1, pp. 52 – 59, 2010.

[43] S. D. Somasundaram, A. Jakobsson, and N. R. Butt, "Countering Radio Frequency Interference in Single-Sensor Quadrupole Resonance," vol. 6, pp. 62–66, Jan. 2009.